공학석사 학위논문

Correlation Between Membrane Fouling and the Ratio of Paticle to Pattern size

패턴과 입자의 크기비가 막오염에 미치는 영향

2014년 8월

서울대학교 대학원
화학생물공학부
장 준 희

Abstract

Correlation Between Membrane Fouling and the Ratio of Particle to Pattern Size

Jun Hee Jang

School of Chemical and Biological Engineering

The Graduate School

Seoul National University

Membrane fouling remains as one of the critical problems which drastically reduce filtration performance of membrane in water and wastewater treatment. Among various studies attempted to solve this problem, patterned membrane has proven the positive effects on membrane fouling. However, the ratio of particle size to pattern size in view point of fouling still remains unclear. In this study, we prepared new nano- and micro-scale patterned membranes and investigated the correlation between membrane fouling and the ratio of particle to pattern size.

Through SEM and AFM imaging, it was confirmed that successful transfer of nano- and micro-scale features with size of 110 nm and 2 μm respectively was made onto the surface of PES UF membrane via hot-embossing NIL method. Although all the membranes have similar pore size, which is approximately 10 nm, regardless of existence of pattern or pattern size, patterned membrane showed 10 – 30 % higher water permeability than flat membrane due to increased effective surface area of patterned surface.

Finally, the effect of particle to pattern ratio on membrane fouling in patterned membrane system was investigated through conducting ultrafiltration of various sized colloidal latex particles. The new parameter, the ratio of particle size to pattern size (R_p), was defined to accurately describe anti-fouling performance of patterned membrane. Also, the extent of membrane fouling was plotted against R_p value and it was found that the range of optimal R_p value was located around 5 when using particles with size from 0.1 to 6 μm. This range of optimal R_p value is expected to provide a useful guide line when selecting effective pattern size to remove specific sizes of foulants in future research or industrial application.

Keywords

Water treatment, Wastewater treatment, Patterned membrane, Nano-scale feature, membrane fouling, Phase inversion, Nanoimprint lithography

Student Number: 2012-20971

Table of Contents

List of Figures

List of Tables

Chapter I

Introduction

I.1. Backgrounds and objectives

There have been technological breakthroughs in wastewater treatment using membrane process over the past three decades, and thereby the volume of wastewater treated with membranes has been significantly increased to satisfy high quality standards and reuse purpose. Especially, a membrane bioreactor (MBR), combination of biological activated sludge process and membrane filtration, has overcome the drawbacks of the sedimentation tank also known as biological treatment system. The membrane processes including membrane bioreactor (MBR), low- and high- pressure membranes separation offer a number of advantages: 1) the contaminants occurring during membrane process can be remove by cleaning the membrane, 2) membrane process is more economical than other competing technologies, and 3) it requires much less area than other alternatives. However, the membrane system still has critical challenge such as membrane fouling, which can be caused by colloids, organic compounds, and microorganisms. The fouling leads to low energy efficiency and a shorter membrane life by repetitive chemical cleaning process. To mitigate fouling problem, various studies have been conducted in engineering, material, and chemistry fields (Drews 2010). Among them, patterning the membrane surface was introduced as a novel approach to control membrane fouling. Although it has been generally accepted that membranes with a rougher surface are more susceptible to membrane fouling, several researchers have reported that patterns on membrane surface can control membrane fouling by promoting shear stress and turbulence near the surface. Won et al. applied the various shapes of pattern on membrane surface and they showed

patterned surface remarkably mitigated the bio-fouling in MBR process (Won, Lee et al. 2012). Anti-fouling effects of patterned membrane have been researched with not only micro-scale pattern but also sub-micro scale pattern. Maruf et al. fabricated sub-micro scale patterned membrane using nanoimprint lithography (NIL) method and reported that less colloidal silica particle and protein were deposited on patterned membrane(Maruf, Rickman et al. 2013, Maruf, Wang et al. 2013). However, patterned membrane did not always show anti-fouling behavior compared to flat membrane. Culfaz et al. prepared the hollow fiber membranes with micro-scale pattern on their surface. It was observed that in dead-end filtrations, although water flux of patterned fiber was 60 % higher than that of flat fiber, filtration resistances caused by fouling were somewhat higher for patterned fibers (Çulfaz, Rolevink et al. 2010). These contradictory claims might be attributed to the fact that anti-fouling effect of patterned membrane depends on several factors such as pattern and foulant size, shape of pattern, hydrodynamic conditions, and feed concentration. More than all, the relationship between pattern size and particle size in view point of fouling still remains unclear, because anti-fouling effect of patterned membranes have been evaluated using the membranes with magnitude-limited patterns. It results from that the regularly ordered patterns could be applied onto membrane surface only at scales from micro to sub-micro until now. In this study, hexagonally well ordered-pattern of nano-scale was prepared by anodized aluminum oxide substrate and applied to PES UF membrane to cover and estimate anti-fouling effect of patterned membrane in nano scale. For comparison study, micro-scaled patterned membrane was also prepared by nano imprinting lithography. These two scales of patterned membranes were tested in

cross-flow system and compared with the flat membrane to confirm correlation between membrane fouling and the ratio particle to pattern size.

Chapter II

Literature Review

II.1 Phase inversion methods.

Since Goetz developed new microfiltration porous membranes with cellulosic materials in the 1960s, phase inversion, interfacial polymerization, track-etching, electro-spinning, and stretching methods have been developed for membrane fabrication. The membranes fabricated by these methods have been used for water and wastewater treatment such as microfiltration (MF), ultrafiltration (UF), nanofiltration (NF), reverse osmosis (RO), forward osmosis (FO), and membrane distillation (MD) (Baker 2000). Table 1 gives an overview of the methods that are commonly used to fabricate polymeric membranes (Lalia, Kochkodan et al. 2013). Among various techniques for membranes fabrication, phase inversion method is the most readily available technique in producing commercial polymeric membranes. In has inversion a polymer solution is transformed from liquid or soluble state to solid state (Drioli and Giorno 2009). This transformation in phase inversion process can be caused by several factors including non-solvent, heat, vapor, and evaporation (Mulder 1996).

- Non-solvent induced phase separation (NIPs): Most commercial membranes are prepared by immersion precipitation. When a polymer solution is immersed in a coagulation bath containing non-solvent, precipitation occurs due to the exchange between solvent and non-solvent.
- Thermally induced phase separation (TIPs): The phase of polymer is separated because of solvation ability of solvent when polymer solution is cooled. After that, the separated solvent is removed by

.

Table 1. Summary of commonly used polymers and fabrication techniques for the preparation of polymeric membranes for water treatment processes (Lalia, Kochkodan et al. 2013).

Water treatment process	Polymers used for membrane fabrication	Fabrication techniques
RO	Cellulose acetate/triavetate Aromatic polyamide Polypiperzine Polybenziimidazoline	Phase inversion Solution casting Interfacial polymerization Layer-by-layer deposition
NF	Polyamides Polysulfone Polyols Polyphenols	Interfacial polymerization Layer-by-layer deposition Phase inversion
UF	Polyacrylonitrile (PAN) Polysulfone (PS) Polyethersulfone (PES) Poly (phthazine ether sulfone ketone) (PPESK) Poly (vinyl butyral) Polyvinylidene fluoride (PVDF)	Phase inversion Solution wet-spinning
MF	PVDF Poly (tetrafluorethylene) (PTFE) Polypropylene (PE) PES Polyetheretherketone (PEEK)	Phase inversion Stretching Track-etching
MD	PTFE PVDF	Phase inversion Stretching Electrospinning

freezing or evaporation.

- Vapor-induced phase separation (VIPs): A casted polymer solution is introduced to a vapor atmosphere which consists of a non-solvent vapor and enough solvent vapor of solution. The membrane is formed by diffusion of non-solvent vapor.
- Evaporation-induced phase separation (EIPs): A polymer solution consists of polymer, solvent and non-solvent where the solvent is more volatile than the non-solvent. Evaporation of non-solvent and solvent causes polymer precipitation.

II.1.1 Non-solvent induced phase separation (NIPs) method

NIPs consists of the following procedures: i) casting of polymer solution onto non-woven fabric layer, ii) immersion of casted polymer solution into a non-solvent coagulation bath, iii)an exchange of solvent and non-solvent, and iv) the formation of polymeric porous membranes by solidification (Boussu, Van der Bruggen et al. 2006). A schematic representation of membrane formation by NIPs is presented in Figure 1. The solvent diffuses into the coagulation bath (as a flux = J_2) while the non-solvent diffuses into the cast film (at a flux = J_1). Demixing takes place with the aforementioned exchange between solvent and non-solvent, and the polymer solution becomes thermodynamically unstable. As a solid polymeric porous membranes with an asymmetric is formed. In this method, UF membranes with pore size of 1-30 nm are obtained when J_2 is much larger than J_1, whereas when J_2 and J_1 are equal, MF membranes with pore size of 0.2 – 0.5μm are formed.

A number of studies have reported that the membrane's pore structure shown by their cross-sectional morphologies depends on several factors such as

polymer, solvent, non-solvent, additives, precipitation time, bath temperature and other parameters during immersion precipitation (Strathmann, Kock et al. 1975, Smolders, Reuvers et al. 1992, Kim, Yoon et al. 2002, Amirilargani, Saljoughi et al. 2010). Thus, polymer's affinity with solvent, mechanical, chemical and thermal properties are of main concern when selecting polymeric building block for membrane. List of commonly applied polymers in membrane fabrication and their advantages and disadvantages are presented in Table 2 (Baker 2000, Liu and Kim 2011).

Among various parameters the concentration of the polymer solution plays a key role in membrane fabrication through immersion precipitation. High polymer concentration solution results in the formation of membranes with low porosity and pore size, which means the macrovoid formation is suppressed. In this cast, sponge-like structure is formed. On the other hand, the Membranes with finger-like structure corresponding with the aforementioned macrovoid can be fabricated with dilute polymer solution. The UF membranes are prepared with polymer solution ranging from 12 wt% to 20 wt%, whereas the support layers of RO membranes are obtained from casting solution over 20 wt% of polymer concentration (Baker 2000).

Selection of solvent and non-solvent is also important in determining properties of membranes such as morphology. The low miscibility of polymer to the solvent causes nonporous membranes, whereas the high miscibility of polymer to the solvent leads to fabrication of more porous membranes. To prepare UF membrane, an aprotic polar solvent including N-methyl-2-pyrrolidone (NMP), dimethyl formamide (DMF), dimethyl acetamide (DMAc), and dimethyl sulfoxide

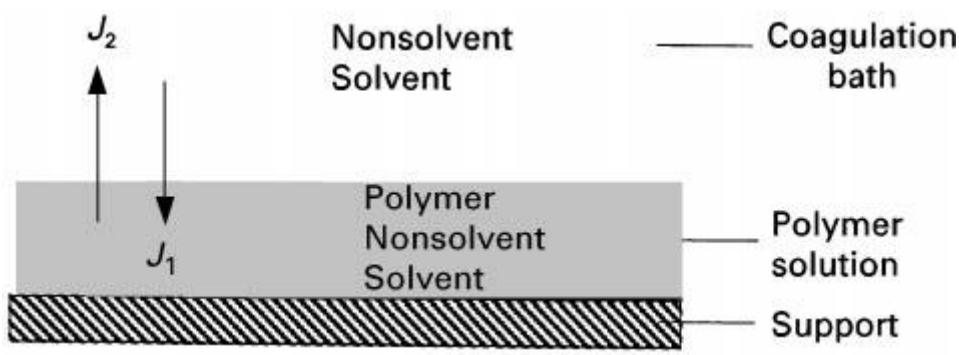

Figure 1. Schematic representation of a film-bath interface. Components : nonsolvent, solvent, and polymer. J_1 is the nonsolvent flux and J_2 the solvent flux (Boussu, Van der Bruggen et al. 2006)

Table 2. Commonly used polymers in membrane formation via immersion precipitation (Baker 2000, Liu and Kim 2011).

Polymer	Advantages	Disadvantages
CA	Hydrophilicity Flexibility in fabrication Low cost	Low thermal resistance (under 30℃) Low chemical resistance (pH 2-8) Poor resistance to chlorine
PS and PES	High thermal resistance (up to 75℃) Wide pH tolerances (1-13) Good chlorine resistance Flexibility in membrane fabrication (wide range of pore size) High mechanical characterisitics	Low operating pressure limits Hydrophobicity
PVDF	High mechanical strength and chemical resistance High thermal stability (up to 75℃)	Hydrophobicity
Polyamide(PA)	Wide pH tolerance High thermal stability High mechanical properties	Poor chlorine resistance

(DMSO) is frequently used. When the polymer solution consisting of polymer and the aforementioned solvents is immersed in non-solvent such as water, demixing rate of these solvents is generally very rapid so that the usage of the solvents leads anisotropic membranes with a high porosity (Pinnau and Freeman 2000).

II.1.2 Evaporation induced phase separation (EIPs) method

Evaporation induced phase separation (EIPs) method is phase separation process induced by evaporation of non-solvent and solvent from initially homogeneous single phase solution. It is also called as dry case process since the change in thermodynamic state of polymer solution is induced without the usage of additional liquid. The evaporation of homogeneous solution leads to formation of two solution phases: polymer lean phase and polymer rich phase. Once evaporation starts, polymer rich phase becomes solid matrix accompanying precipitation. At this point, the region filled with the polymer lean phase develops into pores. The schematic of drying cast process is shown in Figure 2. The pore structure and morphology of membranes fabricated by dry cast process depend on polymer concentration, the ratio of solvent to non-solvent, coating thickness, and evaporation temperature. When the drying rate is high and coating thickness is thin, small pores are formed on top surface. After skin is formed, the non-solvent penetrates through skin and it initiates the macrovoid formation near the skin (Shojaie, Krantz et al. 1994).

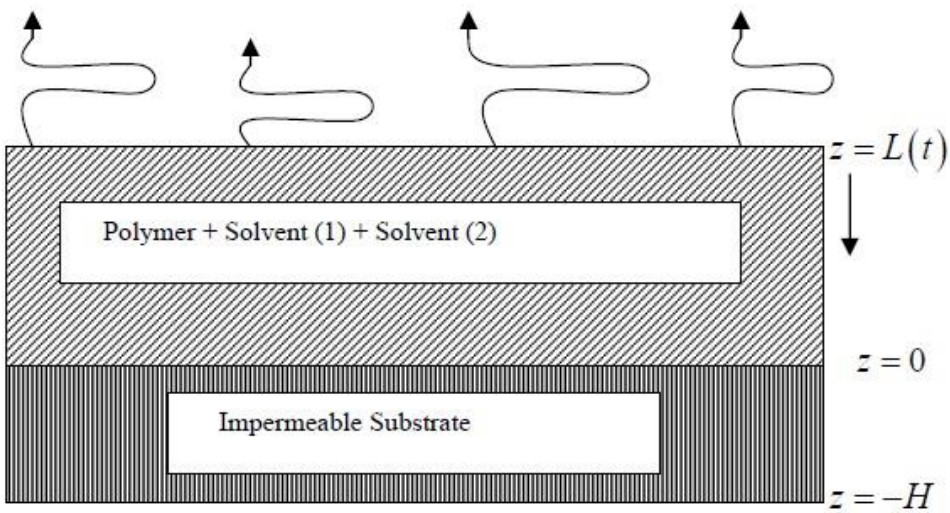

Figure 2. Schematic of evaporation inversion process. (Arya 2013)

II.2 Nano-imprint lithography

Nanoimprint lithography (NIL) is as an alternative to conventional optical lithography because of its low cost, high resolution, and potential for high throughput (Chou, Krauss et al. 1995, Wu, Jung et al. 2005, Kim, Lee et al. 2007, Lee, Hong et al. 2007). Nanoimprint lithography was accepted by International Technology Roadmap for Semiconductor (ITRS) as the next generation lithography candidate, and the number of research papers published has increased as shown in Figure 3. NIL basically a nano-sized stamp with various pattern geometries. In a typical nanoimprint process, this patterned stamp is pressed onto a soft substrate including thermoplastic and UV-curable materials.

II.2.1 Introduction

Nanoimprint lithography is commonly classified into hot embossing lithography, UV-lithography and soft lithography. A schematic and conditions of hot embossing lithography and UV-lithography processes are depicted in Figure 4, Table3, respectively. Regardless of the type of NIL, all the NIL methods goes through the following steps: i) the hard or soft mold with pattern is pressed onto suitable substrate coated with the polymer layer or functional layer with or without heat, and ii) the pattern of mold is transferred due to flow of viscous polymer into cavities of the stamp. The difference between hot embossing lithography and UV-lithography stems from hardening process. The hot-pressed polymer is harden by cooling down below the glass transition temperature in hot embossing lithography, while the UV-curable polymer is solidified with UV lights. After curing the polymer, the imprint mold can be retrieved without damage from patterned

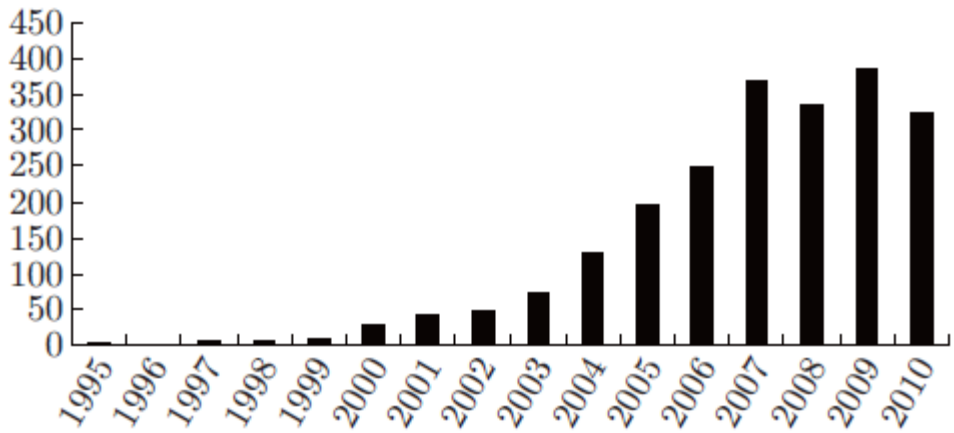

Figure 3. Number of published articles indexed in SCI-E from 1995 to 2010, as a function of year (Zhou, Min et al. 2011)

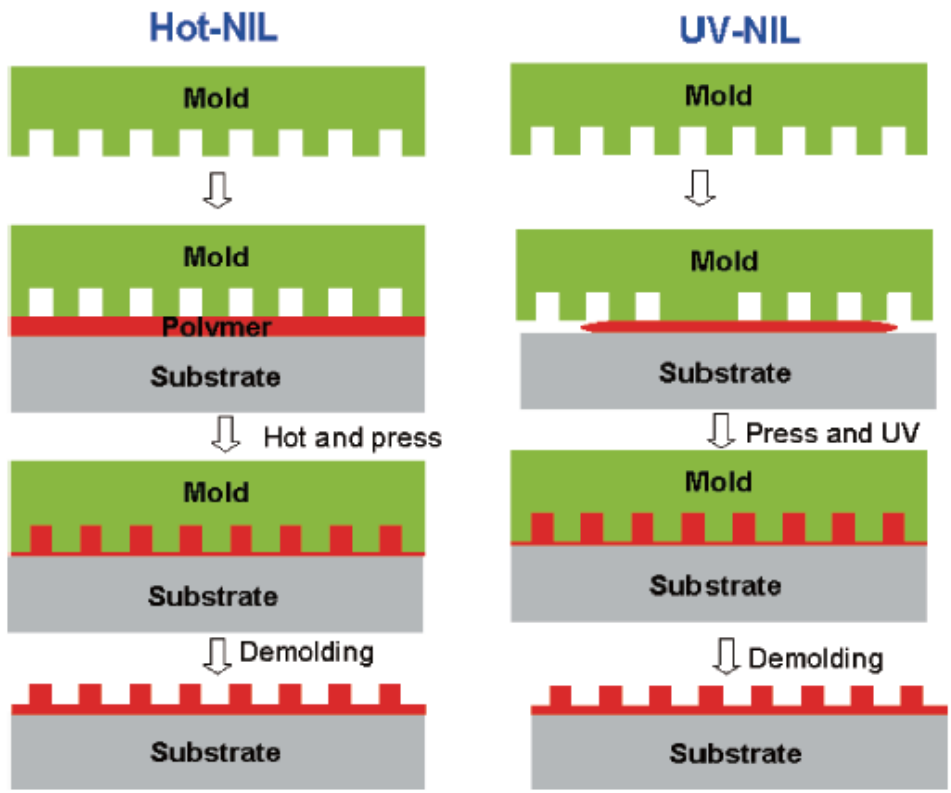

Figure 4. Schematic illustrations for hot embossing and UV-nanoimprint lithography (Zhou, Min et al. 2011).

Table 3. Comparison of thermal NIL and UV-NIL, with typical parameters of current processes (Schift and Kristensen 2010)

Type of NIL	Thermal NIL	UV-NIL
Pressure p	20-100 bar	0-5 bar
Temperature T_{mold}	100-200 ℃	20 ℃ (ambient)
Temperature T_{demold}	20-80 ℃	20 ℃ (ambient)
Resist (polymer)	Solid, thermoplastic Tg ~ 60-100 ℃	Liquid, UV-curable
Viscosity η	10^{3}-10^{7} Pas	10^{-2}-10^{-3} Pas
Stamp area	Full wafer, >200mm diameter	25x25mm2, limited by control of gap
Pressing time	From s to min	<1min (per exposure)
Advantage	Low-cost, large-area equipment and stamps	Low viscosity, low pressure, alignment through mold
Challenge	Process time, thermal expansion due to thermal cycle	Step and repeat needed for large areas
Development needed	Alignment, residual layer homogeneity	Material variety
Hybrid approaches	Thermoset resists: Pressing and curing before demolding	Thermoplastic resist : Hot molding and UV-curing before demolding

polymer and reused for the next molding cycle. Also, the NIL can be divided into hard nanoimprint lithography and soft nanoimprint lithography according to the hardness of mold. Inorganic materials such as SiO_2, Ni, Anodized Aluminum Oxide (AAO), Si, and SiC are used as mold of hard lithography, while organic materials including PDMS, PUA, PVA, PMMA, and PTFE are mainly utilized for soft nanoimprint lithography. Lastly, the NIL can also be sorted into the full-wafer nanoimprint lithography and step-and-repeat nanoimprint lithography according to the imprinted area (Zhou, Min et al. 2011).

II.2.2 Challenges of NIL

Ⅱ.2.2.1 The mold.

In nanoimprint lithography process, the mold is an important determinant of the quality of patterning result is. The mold can be divided into hard molds and soft molds according to the hardness of mold. When hard mold are used in the NIL, they are regularly prepared by electron beam lithography followed by reactive ion etching (RIE). Several groups have recently studied other methods such as two-photon polymerization (Park, Lim et al. 2006) and projection maskless patterning (PMLP) which allows use of thousands of beams in parallel with direct patterning of the substrate (Platzgummer, Loeschner et al. 2007).

Unlike hard molds, soft molds are used for a non-photolithographic strategy (i.e., soft-lithography) based on self-assembly and replica molding for carrying out micro- and nanofabrication. For the soft-lithography, PDMS (Poly-dimethylsiloxane) is the most widely used material as the mold. The micro- and nano-patterned PDMS mold can be prepared by casting the mixture of the liquid PDMS and curing agent on the master molds. After the PDMS mixture is cured, the

patterned PDMS mold can be obtained by peeling them away the master mold.

Regardless of hardness of the molds, the molds used in NIL must be easily detached from the imprinted material without any deformation by strong adhesion between mold and imprinted polymer. To lower surface energy between the mold and imprinted polymer, an anti-adhesion layer or surface treatment of mold is usually applied. Such a layer is normally a self-assembled monolayer of fluorinated silanes (Beck, Graczyk et al. 2002). To reduce the risk of damaging the stamp during the imprint process, it is beneficial to use replicated stamps instead of the original master. Materials for such replicated stamps can be Ormocer-based materials such as Ormostamp (Mühlberger, Bergmair et al. 2009) or polymeric materials not only PDMS but also perfluoropolyether (PFPE) (Huang, Castrataro et al. 2006, Truong, Lin et al. 2007).

Ⅱ.2.2.2 The imprinted polymer materials.

To select a suitable polymer for the NIL process, the following parameters should be considered.

- Adhesion to the substrate. The imprint polymer has to be attached easily to the substrate because it prevents separation between polymer and substrate during the process.
- Non-adhesion to the mold. After curing process, imprinted polymer should be detached easily and clearly from mold maintaining the features of the mold and patterned polymer.
- Functionality. In etching process, the etching selectivity of polymer is higher than substrate (Vogler, Wiedenberg et al. 2007).
- Process compatibility. The imprint polymer must not react with

the mold material.

Ⅱ.2.2.3 The Process.

Since both mold and substrate are not completely flat, the homogeneous contact between mold and substrate is challenging. It mainly results from air trapping at the interface between mold and imprint polymer. Although small air bubbles are less problematic than larger ones for they can dissolve in the imprint polymer, large air bubble persists and reduces pattern fidelity. To solve this problem, a number of approaches have been conducted to bend the substrate of the mold during process using a compliant layer (Bergmair, Mühlberger et al. 2008), flexible stages (Hiroshima 2006), and air cushions (Gao, Tan et al. 2006). Furthermore, controlling the thickness of residual layer in the region where the polymer has been pressed down is also important issue in imprinting process. This layer has to be removed in reactive ion etching process. To optimize the residual layer thickness, the ratio of cavities on the mold to the total mold area must be considered. The thickness of residual layer can become thicker by keeping short time and low pressure, whereas residual layer thickness below tens of nanometer can be obtained by a very elaborate and suitable post-processing. Moreover, mold and substrate distortions can affect the alignment accuracies throughout large areas so that the homogeneity of imprinting pressure is essential for good patterning results (Zhang and Chou 2001). After the imprinting process, the mold has to be detached from imprinted polymer. In this process, the pattern can be deformed or ripped off if the imprinted polymer strongly sticks to the mold or the polymers weakly adhere to the substrate. There are several ways to reduce these damages like detaching at the low temperature by using the mold with low surface energy,

and utilizing flexible mold for easy demolding.

II.3 Patterned membranes

II.3.1 Micro-scale patterned membrane

The concept of patterned membrane was firstly introduced by Wessling group who converged lithography and phase separation method and called it phase separation micro molding (PSμm) (Vogelaar, Barsema et al. 2003). They emphasized that phase separation micromolding is a versatile microfabrication technique and cost-effective process. Using this novel method, a patterned polymeric film was fabricated by the same group. A polymer solution is poured between two substrates containing pattern surface and then exposed to an atmosphere containing water vapor that diffuses through the substrate. By vapor induced phase separation, the micro-perforated polymeric films can be obtained. The morphology is influenced by the thickness of substrate affecting on vapor transport and phase separation kinetics. The preparation step of patterned membrane and membrane morphology are depicted in Figure 5. (Peters, Lammertink et al. 2008, Bikel, Punt et al. 2009).

Micro-scale pattern was applied to hollow fiber as well as flat sheet membrane. Micro-structured hollow fiber for ultrafiltration was prepared using a microstructured spinneret. The surface area of hollow fiber membrane enlarged due to the decrease of the air gap and the increase of the take-up speed and the viscosity of polymer solution (Çulfaz, Rolevink et al. 2010)

Although the patterned membrane developed by Wessling group had merits such as the large surface area, the PSμm method was limited in that dense layer was formed at the opposite side of patterned surface. It means that the

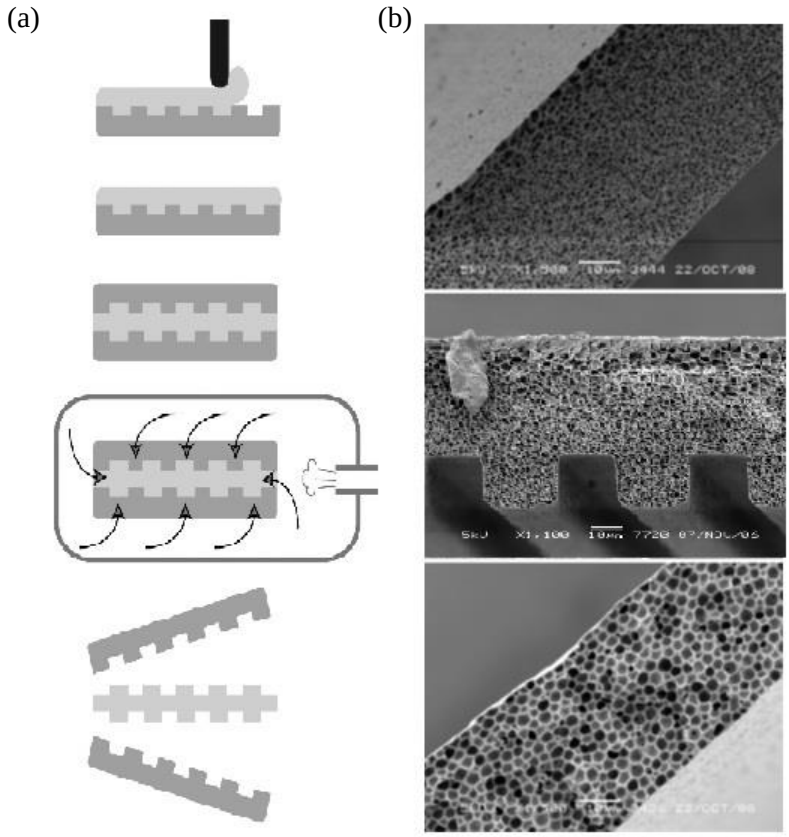

Figure 5. (a) Schematic diagram of preparation of patterned membrane by using PSμm, (b) Cross-sectional images of fabricated patterned membrane (Ç ulfaz, Rolevink et al. 2010).

opposite side of patterned surface plays the role of effective membrane surface. This problem is inevitable because the opposite side firstly contact non-solvent prior to pattern side. In addition, there is limitation to form multidirectional patterns on the membrane surface (Bikel, Punt et al. 2009, Çulfaz, Rolevink et al. 2010). To solve these problems, Lee group reported the patterned membrane fabricated by modified immersion precipitation. According to the modified method, dense layer can be formed on the pattern side so that the pattern side can be used as effective surface during filtration. Moreover, they prepared various patterned membrane including pyramid-, prism-, and embossing-type patterned membranes and compared with them with regard to morphology, permeability, and bio-fouling (Won, Lee et al. 2012). Another solution is surface patterning onto commercial membrane using hot-embossing nanoimprint lithography method (Yildirim, te Braake et al. 2010).

II.3.2 Sub-micro-scale patterned membrane

The pattern size applied on membrane has been studied from micro-scale to nano-scale. First, the pattern size of patterned membrane reported by Wessling and Lee group was micro-scale. They introduced micro-scale patterns on membrane and showed anti-fouling effects of patterned membrane. These effects result from the change in flow near patterned surface induced by micro-scale patterns. Next, Ding group reported that sub-micro patterns can be successfully imprinted on a commercial ultrafiltration membrane surface with hot-embossing nanoimprint lithography method (Maruf, Wang et al. 2013). The morphology of patterned membrane at a micro- and submicro- scale is shown in Figure 6.

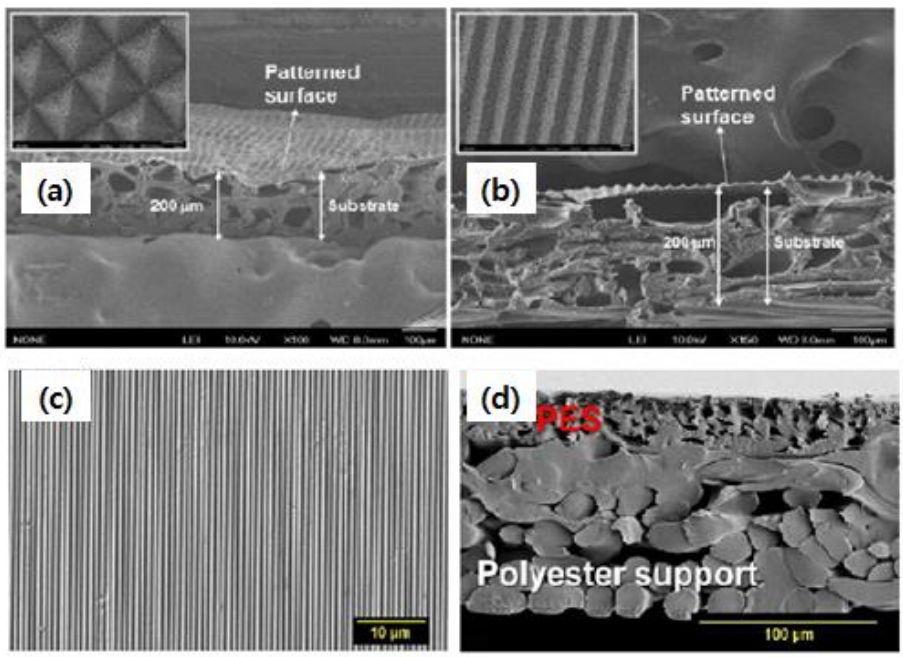

Figure 6. Morphology of micro-scale patterned membrane with (a) pyramid, (b) prism type. (c) and (d) are top- and cross-view of sub-micro patterned membrane

Lastly, the nano-scale patterns aligned on the membrane was also introduced by incorporating nanoparticles in the polymer matrix during phase inversion processes (Jamshidi Gohari, Lau et al. 2013). Although they reported that nano-sized pattern was successfully fabricated with nanoparticles, characteristics such as the morphology of pattern surface still remains unclearly because they showed only AFM images of the membrane with nano-scale patterns.

II.3.3 Correlation between membrane fouling and roughness of membrane surface

Several surface characteristics of membranes including charge, hydrophilicity, and roughness are known to mainly influence the fouling since they determine the interaction between the membrane and foulants (Committee 2005). Among them, the correlation between membrane fouling and roughness of membrane surface has been studied and it has been generally accepted that membranes with a smoother surface are less susceptible to membrane fouling. The effect of surface roughness on degree of flux decline was investigated using two NF and two RO membranes (Vrijenhoek, Hong et al. 2001). They demonstrated that fluxes decrease with the increase in the surface roughness of the membrane during filtration of colloidal silica particle solution. This decrease in flux according to the increase in surface roughness is attributed to the increase in the total surface area onto which foulants can be attached and the ridge-valley structure which can cause entrapment of foulants at the surface. Similar observation was made with six different NF and RO membranes by Hobbs et al (Hobbs, Hong et al. 2006). In this study, the ratio of three dimensional area to two dimensional area was defined as

the surface area difference, where the rougher surfaces have higher surface area difference. The results indicated that membrane fouling became more severe with the increase of surface area difference. A linear correlation between surface roughness and membrane fouling also appeared in MF and UF membranes. Kang et al. reported that initial cell deposition rate was correlated with surface roughness with a linear correlation factor of 0.79 (Kang, Hoek et al. 2006).

Conversely, Riedl et al. reported that rougher surfaces on membrane have advantage in flux decline (Riedl, Girard et al. 1998). They examined flux behavior of four different membranes during dead-end microfiltration of commercial apple juice. PES and PVDF which have rough surface produced a looser surface fouling layer that has a lower flow resistance per unit thickness of foulant and higher overall fluxes than the dense fouling layers observed on smooth surfaced membranes. Moreover, cleaning agents would more easily penetrate a looser fouling structure, making rough surfaced membranes easier to clean.

II.3.4 Fouling behavior on patterned membranes

Although rougher surfaces have higher fouling tendency as mentioned previous section, surface patterning has been reported to mitigate the attachment and growth of biological cells which are foulants in membrane process (Chen, Mrksich et al. 1997). These anti-fouling effects of surface patterns have been studied in membrane system as well as non-membrane system. Recently, the various types of pattern were applied on membrane surface using modified phase inversion method and mitigation of biofouling on patterned membrane was investigated, by Won et al.. They tested adhesion of microorganisms on patterned and flat membrane using activated sludge at Reynolds number (*Re*) ranging from

1100 to 1200 and reported that the patterned surface substantially mitigated the biofouling comparing with flat membrane (Figure 7). This was attributed to shear effect and local turbulence, which was induced by the patterned surface.

The fouling reduction on sub-micro patterns has also been proven by Ding group. As written in previous section, they introduced sub-micro scale patterns on a commercial UF membrane using NIL method. The patterned membrane with sub-micro scale patterns showed superior anti-fouling property in colloidal silica particle filtration test, which was evidenced by increase in the critical flux. In following paper, the same patterned membrane with bovine serum albumin (BSA) was used to confirm its resistance to protein fouling. The test revealed less protein deposition on the patterned membrane than that on pristine membrane. In this research, the effects of correlation between directions of feed flow and pattern orientation were discovered as follow: and BSA fouling can be mitigated when the feed flow direction is perpendicular to the pattened lines.

However, patterned membrane did not always show anti-fouling behavior compared to flat membrane. The fouling behavior of hollow fibers with micro structure on their surface was reported by conducting dead-end filtration test with colloidal silica and sodium alginate. In this paper, it was observed that in dead-end filtrations, although water flux of patterned fiber was 60 % higher than that of the flat fiber, filtration resistances caused by fouling were somewhat higher in patterned fibers (Çulfaz, Buetehorn et al. 2011).

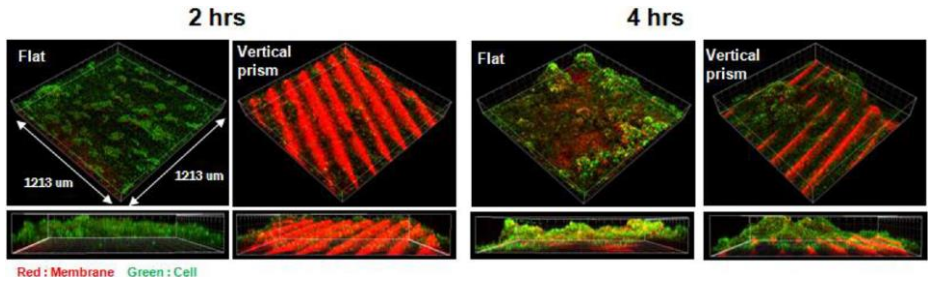

Figure 7. CLSM images of the used flat sheet and prism-patterned membranes after 2 and 4 hr operation in the cross-flow MF of the mixed liquors taken from MBR.

Chapter III

Material and Methods

III.1 Fabrication of the pattern molds

III.1.1 Micro-scaled pattern mold

The Micro-scaled pattern mold was prepared as follows. Polished silicon wafer (100, p-type) was cut into 3 cm X 3 cm pieces and cleaned with isopropanol and acetone. Wafer substrates were treated with UVO for 1 min to increase hydrophilicity of the wafer surface. A 10 wt% aqueous suspension (Sigma Aldrich) consisting of the polystyrene latex beads with a diameter of 2 μm was diluted with ethanol (polystyrene solution:ethanol = 1:5) and sonicated for 1 hr to improve dispersibility of the particles. 50 μl of the diluted PS solution was dropped onto the surface of water, resulting in the self-assembly of PS latex beads and 10 μl of 2 wt% dodecylsodiumsulface (SDS, Sigma Aldrich) solution was added to water to make rigid PS latex beads monolayers.

Using the scooping transfer technique, PS monolayer array was transferred from the surface of water to the wafer substrate surface (Figure 8-1). After dried at room temperature, the hexagonally packed PS beads array on wafer was prepared. To obtain replica of highly ordered template, the Poly (dimethylsiloxane) (PDMS) prepolymer (base:curing agent = 10:1, Slygard 184, Dow Corning) was thoroughly mixed and then poured onto the template. The prepolymer was cured for four hours at 60 ℃ in a convection oven. The cured micro patterned PDMS was peeled from the PS beads template (Figure 8-3).

Positive-patterned template was prepared by transferring negative-pattern of PDMS template using UV-curable polymer, Poly (urethane acrylate) (PUA,

311RM, Minuta Tech.). A few drops of PUA was dropped on the positive-patterned PDMS and Poly (ethylene terephrhalate) (PET) film was placed on the PUA drops. The PUA drops was cured by exposing it to UV light (λ: 360±20nm, MT-GJ20 Minuta Tech.) for 10 min. After finishing curing step, the negative-patterned PUA template was released from PDMS mold and exposed to UV light for 12 hr again (Figure 8-4). To fabricate negative-patterned PUA template, replication step was repeated. This step was the same with previous step except for using wafer as the support of PUA instead of PET. Lastly, micro-sized and negative patterned PUA mold on wafer was prepared (Figure 8-6).

III.1.2 Nano-scaled pattern mold

Nano-scaled pattern mold was prepared with anodized aluminum oxide (AAO). The highly ordered anodic aluminum oxide (AAO) templeate was fabricated by two-step anodization. Aluminum sheet (99.999%, Goodfelllow) was cut into 2X5 cm pieces and electro-polished chemically in a solution of mixture of 4:1 ratios of ethanol and per-chloric acid to provide a smooth surface. Afterwards, the Al was anodized in 0.3 M oxalic acid solution at constant 40 V and 15 ℃ for 12 hr. After this first anodization step, the template was immersed in a chromic acid and hydrochloric acid mixture to remove porous aluminum oxide layer. Subsequently, the second anodization was repeated in the same conditions with previous anodization step for 100 s, and then the sample promptly rinsed with ethanol and distilled water. To wide pore diameter of AAO, the porous AAO was immersed in 0.1 M phosphoric acid solution at 30 ℃ for 30 min.

The modification of end-functional group of the AAO template to

monoglycidyl ether-terminated poly (dimethylsiloxane) (PDMS, Mn=5,000, Sigma Aldrich) was performed on the surface of the nanoporous AAO template in order to easily detach membrane from the AAO template due to hydrophobic characteristics. All the processes are depicted in Fig 9.

III.1.3 Non-patterned mold

Non-patterned mold which has the flat surface was prepared to compare with micro- and nano- patterned UF membranes. The 2 by 2 cm pieces of silicon wafer (100) was treated with PDMS solution at 80 ℃ for 4 hr to low the surface energy of template.

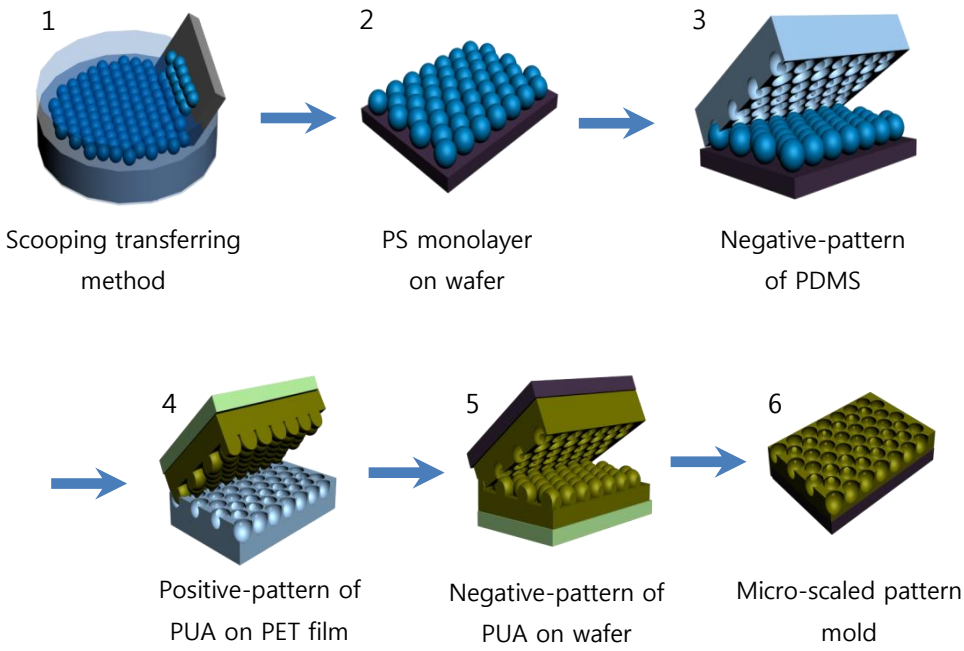

Figure 8. Fabricating steps for micro-scaled pattern mold

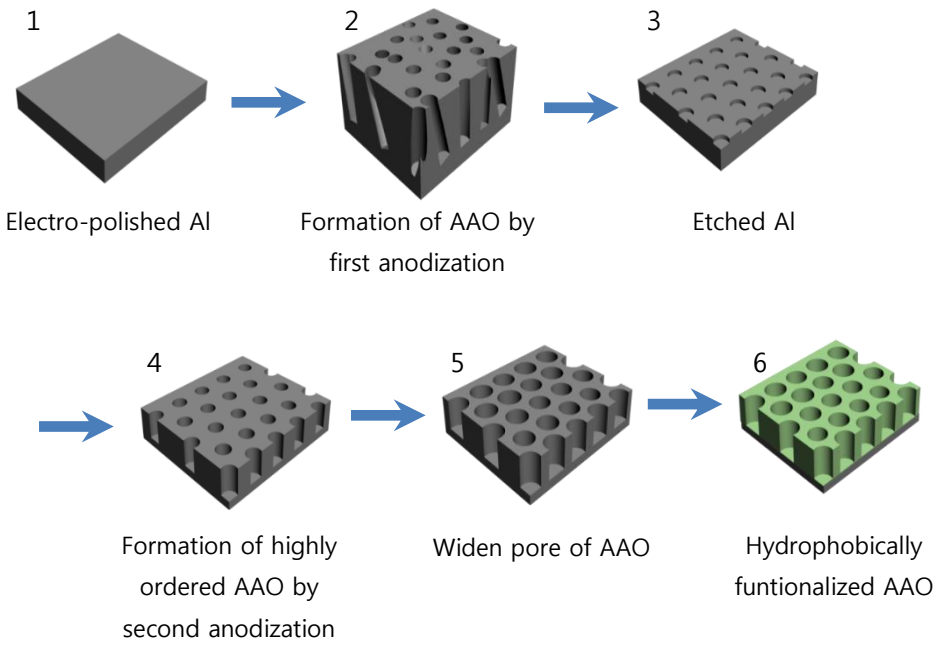

Figure 9. Fabricating steps for nano-scaled pattern mold

III.2 Preparation of patterned membranes

III.2.1 Dried PES UF membrane

Poly (ether sulfone) ultrafiltration membrane was prepared by conventional non-solvent induced phase separation (NIPS) method. First of all, PES powder (Basf) in the amount corresponding to 15 wt% was dissolved in N-methyl-2-pyrrolidone (NMP, Sigma Aldrich) by stirring for 8 hr at 60 ℃, and cooled to room temperature without agitation. The homogenous solution was casted onto the non-woven fabric substrate by using casting knife set at a gate height of 150μm. The casting film on substrate was coagulated in a deionize water for 24 hr for the purpose of entire liquid-liquid demixing. Since the porous structure of wet membranes can be collapsed during imprinting pattern mold on membranes with heat, dehydration process is required to get dried membrane. Bansod et al. showed membrane could be dehydrated by dipping wet membrane in 50 wt% glycerol (Sigma Aldrich) aqueous solution for one day and was dried at room temperature for another one day to remove water (Bansod, Sapkal et al. 2012).

III.2.2 Patterning process

A schematic diagram of the patterning process on the membrane was depicted in Figure 10. The patterning was conducted using hot-press equipment (V-SYSTEM, Korea). The prepared pattern and non-pattern mold were placed on the dried membrane, and then pressed at 4 MPa and 150 ℃ for 5 min. Lastly, the mold was released from the membrane at 20 ℃ DI water.

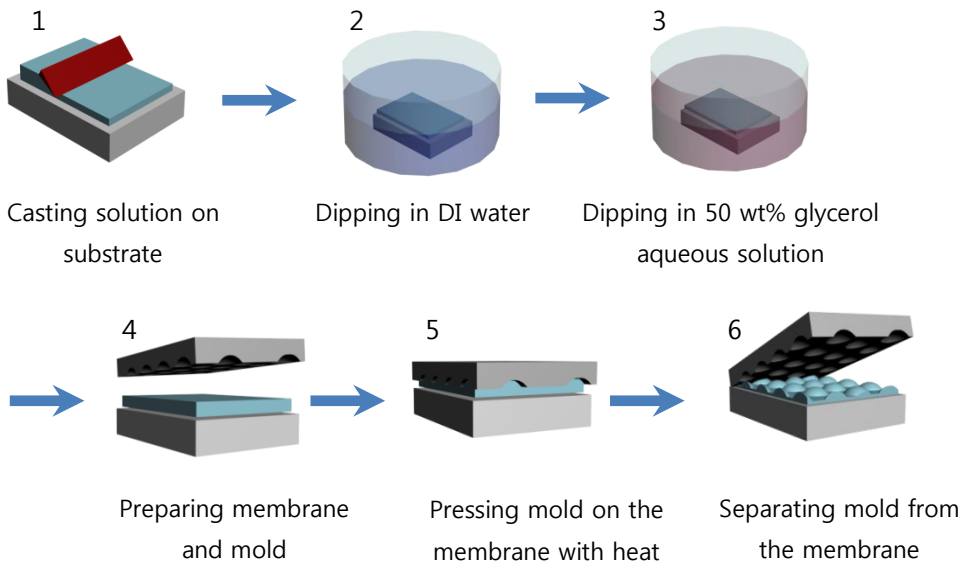

Figure 10. Preparation of patterned membranes

III.3 Characterization of patterned membranes

The top surface and cross-sectional morphologies of the patterned and non-patterned membranes were observed by a Scanning Electron Microscope (SEM, JSM-6701F, JEOL, USA). All the membranes were investigated by SEM after coated with gold-platinum by a sputter coater. The effective surface area of patterned and non-patterned membranes was measured by an atomic force microscopy (AFM, Nanonavi, Japan).

The mean pore sizes of the membranes were calculated from the molecular weight cut-off data with poly (ethylene oxide) and poly (ethylene glycol). Poly (ethylene glycol) (PEG, Sigma Aldrich) with average molecular weights of 1, 10, and 35 kDa and Poly (ethylene oxide) (PEO, Sigma Aldrich) with MWs of 100, 200, and 300 kDa were used as solute for solute transport tests. The test solution was prepared by dissolving PEG or PEO in distilled water at a concentration of 1000 ppm. After each membrane was compacted at 400 kPa for 2 hr, ultrafilration experiments were conducted by using dead-end stirred cell with an effective area of 1.76 cm^2. The operational pressure, the rate of agitation, and filtration time were 300 kPa, 200 rpm, and 2hr, respectively. The PEG and PEO concentration in the feed and in permeate were measured by using a total organic carbon analyzer (Seivers 5010C, GEAI).

III.4 Filtration performance of patterned membranes

To evaluate performance of patterned and non-patterned membranes, each membrane was operated in cross-flow ultrafiltration system (Figure 11). The test cell was 22 X 22 mm in length and width and 2 mm in depth with an effective area of 4 cm^2. All the membranes were compacted for 2 hr at 400 kPa prior to filtration test.

III.4.1 Pure water flux test

The pure water flux of non-, nano-, and micro- patterned membranes was measured by continuously permeating deionized water at the constant pressure, increasing gradually from 100 kPa to 400 kPa every 50 kPa. The pure water permeate was obtained every 5 min for the four steps.

III.4.2 Filtration of colloidal particles

In colloidal filtration test, 2.5 wt% aqueous suspension of polystyrene latex microspheres (Alfa Aesar) with diameters of 0.1, 0.5, 2 or 6 μm were used. Prior to the filtration test, the feed suspensions were sonicated for 1 hr and stored at room temperature. To confirm quantitatively degree of particles aggregation during the filtration experiments, these suspensions were examined with particle size analyzer (Photal, Korea) every 30 min (Figure 12). These feed solutions were used in filtration measurements at linear velocity of 0.4 cm/s. All the filtration conditions were summarized at Table 4.

After the cross flow system operation, patterned or non-patterned membranes was immersed in DI water and sonicated for 1 hr to detach particles deposited on the membranes. The mass of detached particle can be calculated by

measuring absorbance of particle dispersion solution with spectrophotometer (Mechasys, Korea). To determine optimum wavelength at which absorbance of particle solution is the largest, absorbance of diluted particle solution were measured at the wavelength ranging from 200 nm to 1000 nm for every 50 nm and the results were shown in Figure 13. The calibration curve between concentration of detached particle solution and absorbance was illustrated in Figure 14. These curves were obtained at which the wavelength had the highest value of absorbance; 300 nm for 0.1 and 0.5 μm particle, 750 nm for 2 μm particle, and 900 nm for 6 μm particle.

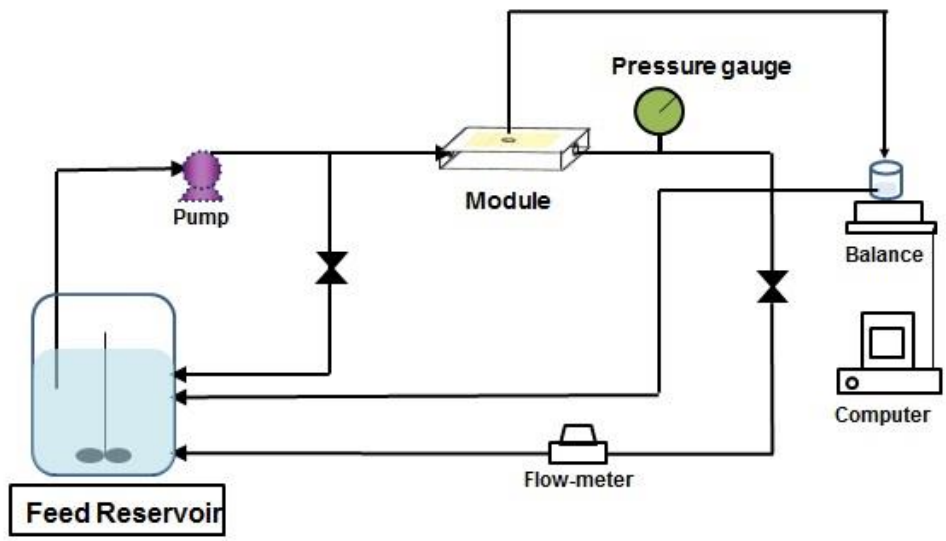

Figure 11. Schematic diagram of ultrafiltration cross-flow system.

Table 4. Conditions PS colloidal filtration test.

Temperatuer	25 ~ 27 ℃
pH	6.4-6.8
Compaction pressure	400 kPa
Compaction time	2 hr
Colloidal filtration pressure	200 kPa
Colloidal filtration time	2 hr
Particle size	0.1μm 0.5μm 2 μm 6 μm
Feed concentration	0.8 ml particle solution / 1 L DI for 2, 6 μm 0.2 ml particle solution / 1 L DI for 0.5 μm 0.04 ml particle solution / 1 L DI for 0.1 μm
Linear velocity	0.4 ~0.5 cm/s (Re 14 – 16)
Stirring speed	200 rpm

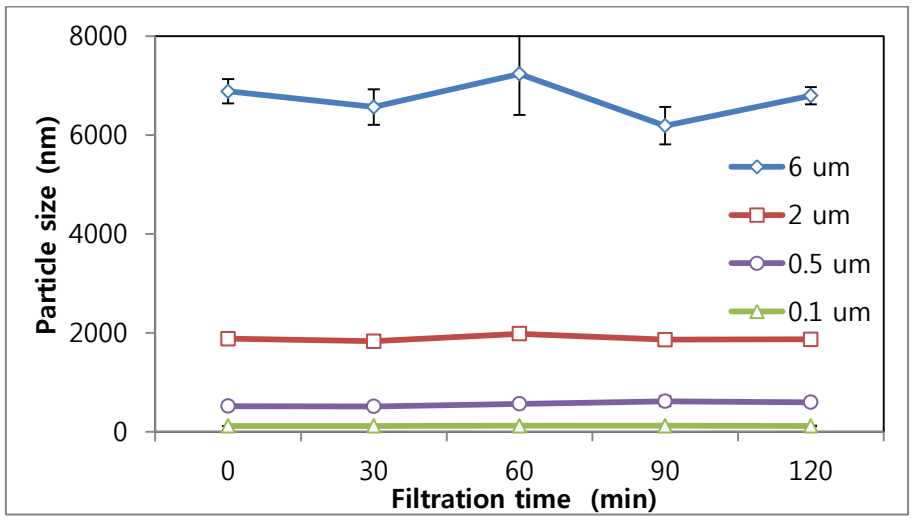

Figure 12. Particle size average during colloidal filtration test.

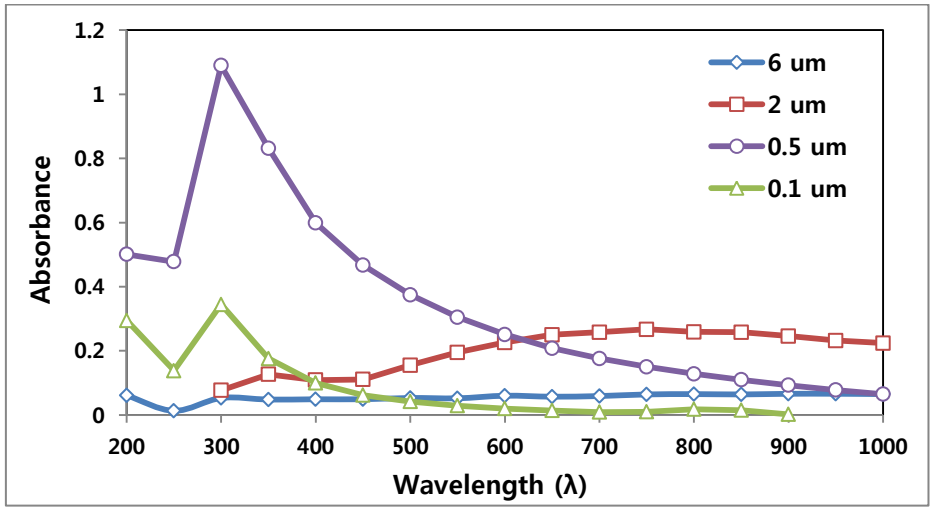

Figure 13. Absorbance of particle suspensions according to wavelength.

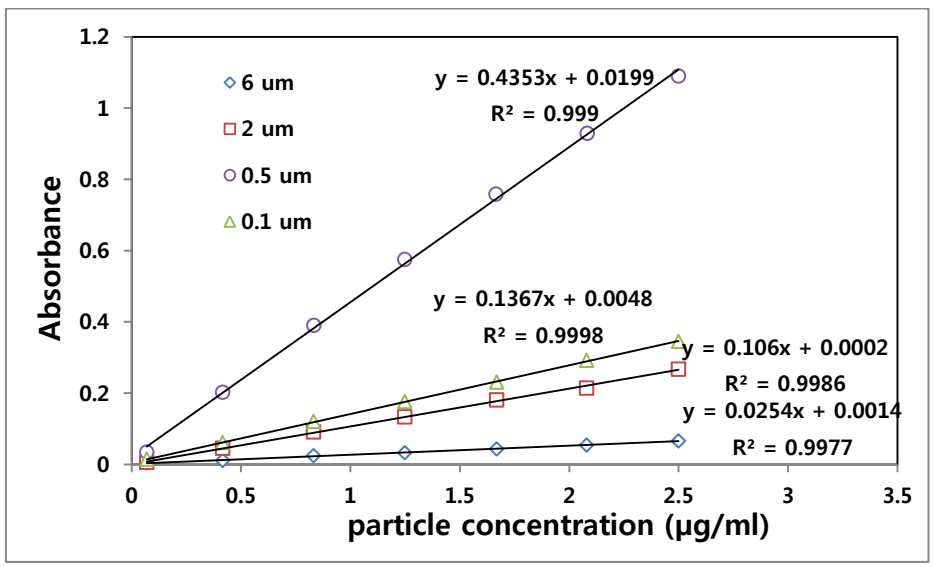

Figure 14. Calibration curves between particle suspensions concentration and its absorbance in spectrophotometer.

Chapter IV

Results and Discussion

IV.1 Observation of the pattern molds

From hexagonally packed PS beads monolayer array on wafer, micro-scale pattern mold was successfully obtained through a couple of pattern transferring process. Figure 15 (a) and b show top-view and cross-sectional SEM images of micro-scale pattern mold, respectively. The micro-scale pattern transferred on membrane surface the diameter of 1.9 – 2.1 μm and the depth of 0.5 – 0.6 μm. Little decrease in pattern diameter and depth is caused by incompletely penetration of PDMS polymer into PS monolayer.

A densely packed hexagonal pore structure and anodized aluminum oxide (AAO), fabricated by two step anodization method is known as attractive template due to their relatively easy and low-cost processing (Masuda and Fukuda 1995). In this study, nano-scale porous alumina grown in 0.3 M oxalic acid electrolyte was used as nano pattern template and the nano pattern template had pores with a diameter of 100 nm (Figure 15-c,d).

Flat mold was prepared to fabricate non-pattern membrane for the purpose of proving pattern effects. The top surface of modified wafer was flatter than that of pattern mold as shown SEM image (Figure 15-e).

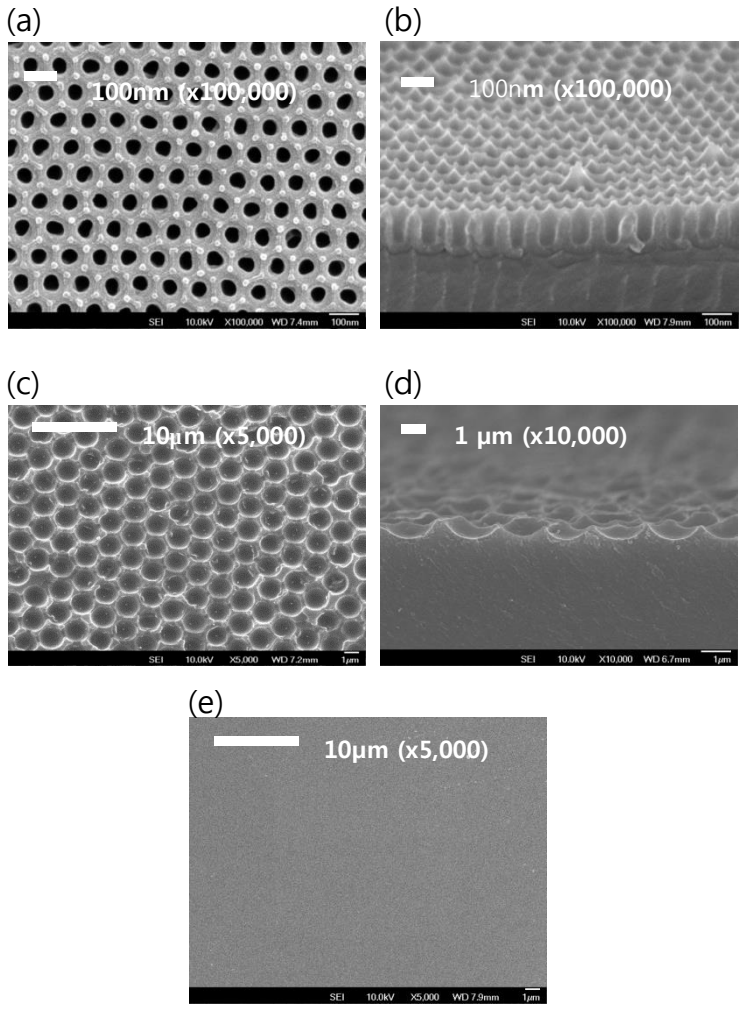

Figure 15. SEM images of pattern mold in a nano-scale (a) top-view, (b) cross-view, micro-scale (c) top-view, (d) cross-view, and non-patterned mold (e) top-view.

IV.2 Observation of pattened membrane morphology

IV.2.1 Dried-PES UF membrane

The polyethersulfone ultrafiltration membrane with porous finger-like structure was prepared using conventional immersion precipitation method. The formation of the porous finger-like structure results from instantaneous demixing of polymer solution, and is associated with mass transfer during phase inversion process (Reuvers and Smolders 1987). Prior to pattering of the PES UF membranes, the membranes were dehydrated by filling pore with glycerin instead of water to minimize possible pore collapse during patterning.

IV.2.2 PES UF membrane with micro- and nano-scale pattern

In the literature review section, the hot-embossing NIL process was described as a simple and well-known technique capable of fabricating sub-10 nm feature. A typical method for thermal embossing is that a polymer film is squeezed into the cavities of pattern mold at a temperature above the transition temperature (T_g) of the polymer under high pressure. After molding, pattern mold is peeled off from a replica at a temperature below T_g. However, the conventional thermal embossing method which is operated at a higher temperature than T_g could cause collapse of porous structure during imprinting of UF membrane (Maruf, Wang et al. 2013). Although patterns can be completely transferred using hot embossing method, it is obvious that the irreversible collapsed pore of membrane is not desirable to water permeation. To achieve successful imprinting on membrane without sacrificing permeability, Maruf et al. suggested carrying out the NIL patterning of the UF membrane at a temperature below the T_g of the polymer.

Nevertheless, height of patterns imprinted on membrane was smaller than the depth of the mold when imprinting at a lower temperature than T_g.

To maintain porous structure, the imprinting process at a 150 ℃ which is below T_g of PES polymer (185 ℃) was conducted. The nano- and micro-scale pattern imprinted on the UF membrane is revealed in Figure 17-b1 and c1. Also, Figure 17-3 and -4 represent the topographic AFM images of patterned and non-patterned membranes. From these images, it was confirmed that thicknesses of nano- and micro- patterns were 20 – 30 nm and 400 – 500 nm, respectively. Moreover, pattern size is defined as a distance between valleys of pattern. The pattern size of each membrane is 90 - 110 nm and 1.9 – 2.1 μm respectively. Since the membranes are imprinted under high pressure (4 MPa), finger-like structure of all the membranes are a little deformed regardless of existence of pattern as observed in cross-sectional SEM images (Figure 17-2.)

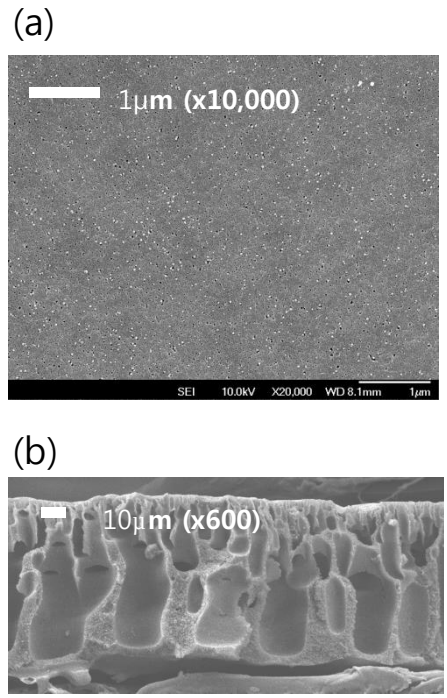

Figure 16. PES UF membrane fabricated by NIPs method (a) top-view and (b) cross-sectional image.

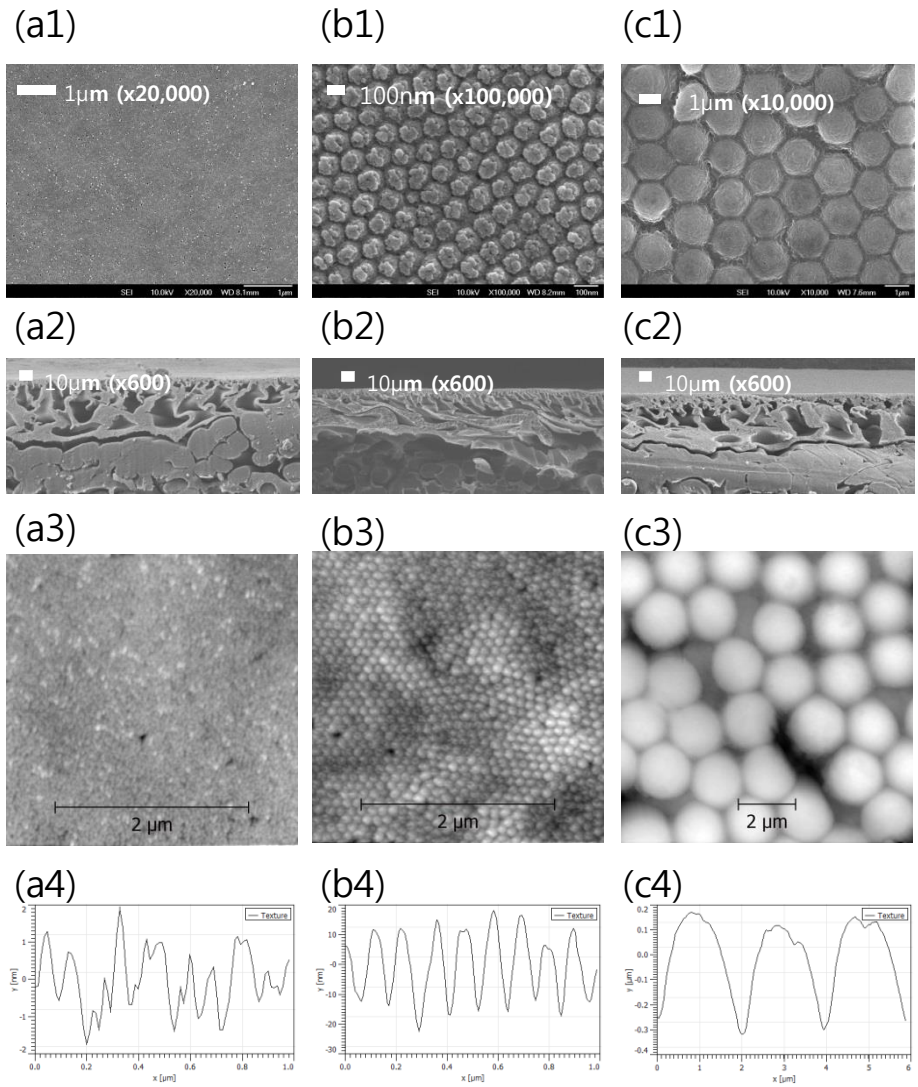

Figure 17. SEM and AFM images of patterned and non-patterned membranes. (a) indicate non-patterned membrane and (b) and (c) represent nano- and micro- patterned membranes, respectively

IV.3 Surface area of patterned membranes.

Average roughness values and effective surface area of each membrane (n=5) were measured by AFM and calculated using Gwyddion SPM data analysis software. AFM images show that non-patterned membrane has a relatively smooth surface with a roughness of only 1.05 nm in a 3 μm X 3 μm area (Table 5). In contrast, applying patterns to the membrane surface results in a dramatic increase in roughness value to 4.80 and 114 nm for nano-pattern and micro-pattern, respectively. The relative surface area of each membrane corresponding to ratio of effective surface area to projected area is also tabulated in Table 5. The value of effective surface area is the same regardless of pattern size as long as pattern shape is identical. Although the shape of micro-patterned membrane was the same with that of nano-patterned membrane, however, relative surface area of mico-patterned membrane was larger than that of nano-patterned membrane because micro-pattern had larger the ratio of height to diameter than that of nano-pattern.

Table 5. Relative surface area and roughness value of non-patterned and patterned membranes.

	Non-patterned membrane	Nano-patterned membrane	Micro-patterned membrane
Relative surface area	1.003 ± 0.002	1.078 ± 0.028	1.158 ± 0.08
Roughness value (nm)	1.054 ± 0.282	4.803 ± 0.407	114 ± 36.4

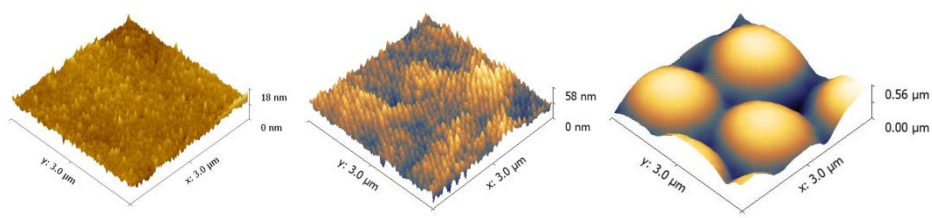

IV.4 Pore size of patterned membranes.

IV.4.1 Molecular weight cut-off

Among various methods to represent flux and rejection characteristics of asymmetric ultrafiltration membranes, molecular weight cut-off (MWCO) has been used to analyze membrane selectivity for solute molecules of different molecular weights. The MWCO value is molecular weight of solute at which 90% rejection can be achieved where rejection is defined as in equation 1:

$$\text{Rejection, R (\%)} = \left(1 - \frac{C_p}{C_f}\right) X\ 100 \qquad (1)$$

where C_p and C_f are the concentration of permeate and feed, respectively.

As shown in Figure 18, the MWCO of each membrane was determined using PEG and PEO. The MWCO of micro-patterned membrane was determined to be 100.1 kDa, which was slightly higher than that of non-patterned membrane, 95 kDa. It is inferred that the pores on membrane surface which contact with micro-pattern mold could be slightly deformed by lateral tension during imprinting process. However, nano-patterned membrane had similar MWCO value with non-patterned membrane because tension on membrane surface was negligible due to small size of nano-pattern.

IV.4.2 Pore size calculation from MWCO

The relationship between the solute rejection and the size of solute has been treated by many researchers to obtain information about mean pore size and pore size (Michaels 1980, Kassotis, Shmidt et al. 1985, Aimar, Meireles et al. 1990). Michaels et al. found that the sieving coefficient of ultrafiltration membrane

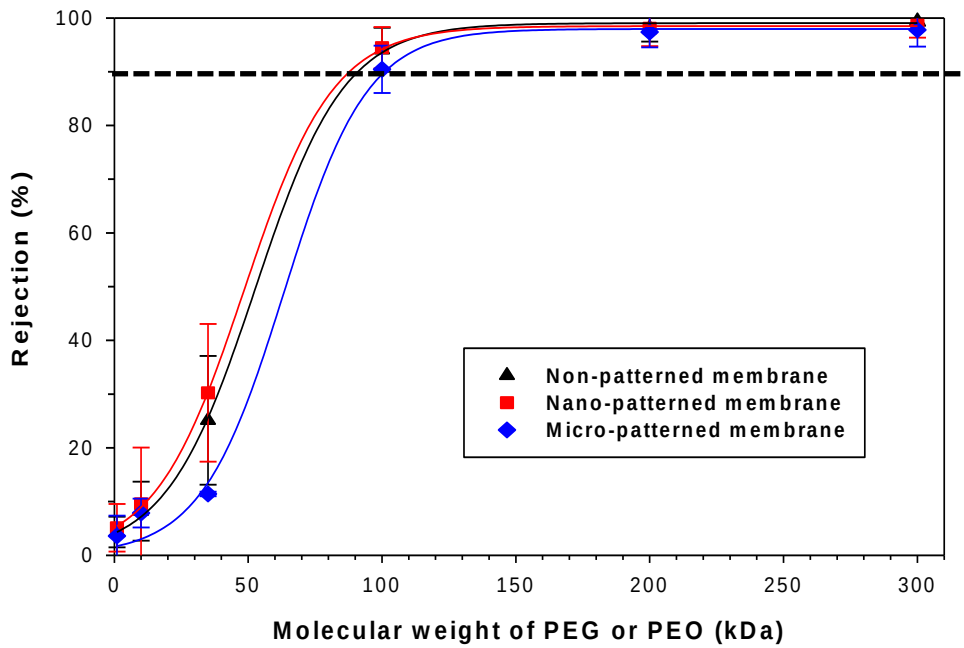

Figure 18. Molecular weight cut-off of patterned and non-pattrned membranes.

to the solute size remarkably fit to a log-normal probability distribution curve. Also, when solute rejection (R, %) is plotted as a function of the solute diameter (d_s) on a log-normal probability paper, a straight line is obtained and can be expressed as equation 2.

$$R = A_0 + A_1(\ln d_s) \quad (2)$$

From this log-normal plot, mean solute size can be calculated as ds corresponding to the solute separation of 50%. The mean pore size of the membrane can be regarded to be the same with solute mean size, by ignoring the influence of solute rejection caused by the steric and hydrodynamic interaction between solute and pore (Michaels 1980).

The Stokes radius (a) of macromolecule can be obtained from Stokes-Einstein equation. In case of PEG and PEO, Stokes radius, a (cm), is calculated following equation 3 and 4, respectively.

$$a\ (PEG) = 16.73 \times 10^{-10} M^{0.557} \quad (3)$$

$$a\ (PEO) = 10.44 \times 10^{-10} M^{0.587} \quad (4)$$

where M is molecular weight of solute(Singh, Khulbe et al. 1998).

From these theories, mean pore size of each membrane is calculated in plot of solute rejection as a function of solute radius on log-normal probability paper. The mean pore sizes of nano- and non-patterned membranes are similar, 8.3 nm, which are lower than that of micro-patterned membrane, 9.9 nm (Figure 19). It is because micro-patterned membrane has higher MWCO value than others.

MW (kDa)	1	10	35	100	200	300
Stokes diameter(nm)	1.569	5.656	11.37	17.98	27.00	34.26

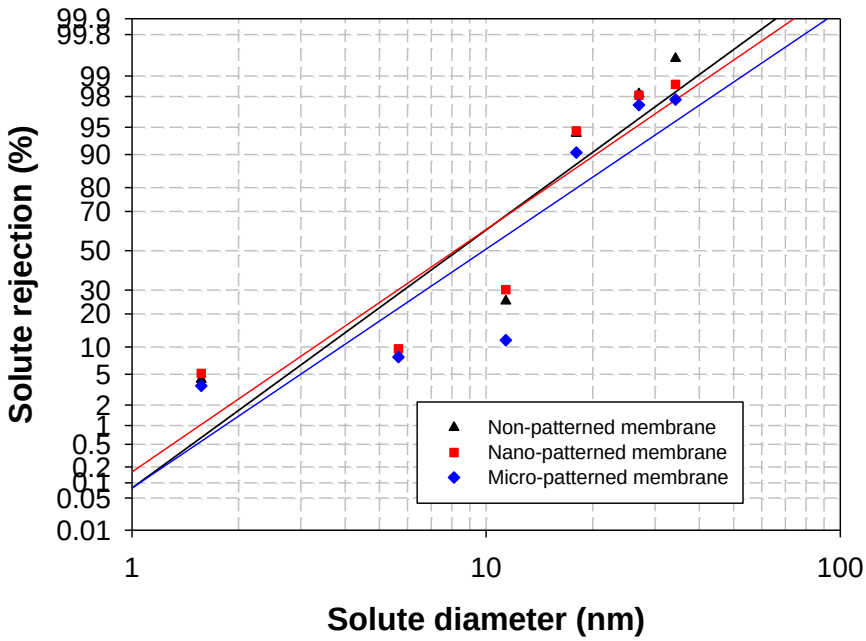

Figure 19. Plot between solute rejection and solute diameter on log-normal probability paper with patterned and non-patterned membranes

IV.5 Pure water filtration of patterned membranes.

To evaluate water flux of all three membranes, three kinds of membranes with nano-scale patterned, micro-scale patterned and non-patterned membranes were prepared. The plots of water permeability obtained in cross flow system as a function of pressure are shown in Figure 20. Micro- and nano-patterned membranes revealed higher water flux performance than non-patterned membrane. These results can be attributed to 1) effective surface area (Table 5) and 2) mean pore size (Figure 19) of the membrane. As effective surface area of nano-patterned membrane was similar with that of flat membrane, increase in water flux of nano-patterned membrane might be due to higher surface area of the membrane. Furthermore, water flux of micro-patterned membrane was enhanced by slightly higher pore-size and effective surface area.

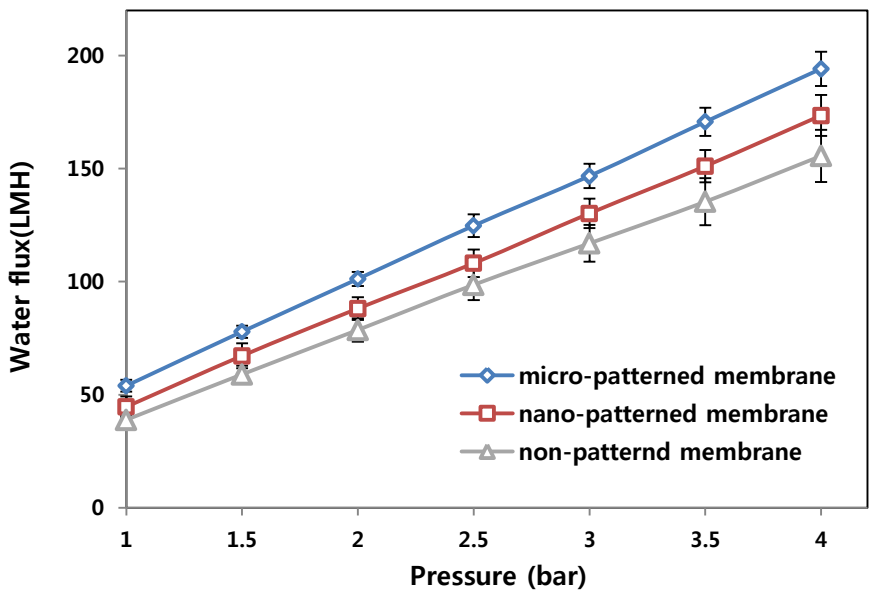

Figure 20. Pure water filtration of patterned and non-patterned membranes.

IV.6 Selection of particle size.

Before conducting colloidal particle filtration test, suitable particle size which can be deposited on membrane surface in cross-flow system has to be determined. Effective particle velocity, which is closely related with particle size, is composed of permeation velocity and overall back transport velocity. Particle transport toward the membrane is affected by the drag forces associated with the axial and lateral (permeation) directions of fluid flow. However, particles can be delivered from the membrane due to several forces including diffusion induced by concentration polarization, shear induced diffusion, lateral migration due to fluid inertia, and sedimentation as shown in figure 21. To calculate each velocity in flat sheet membrane, we used following equations.

Gravity (V_R) = $\frac{\pi}{18\eta} {d_p}^2 \rho_p g$ (1)

Buoyancy (V_{BU}) = $\frac{\pi}{18\eta} {d_p}^2 \rho_l g$ (2)

Brownian diffusion (V_B) = $\frac{kT}{3\pi\eta d_p \delta}$ (3)

Shear-induced diffusion (V_S) = $0.0225 \frac{u_0 {d_p}^2}{h\delta}$ (4)

Lateral migration (V_l) = $0.1078 \frac{\rho_p {u_0}^2 {d_p}^3}{\eta h^2}$ (5)

Leveque's equation : $\frac{d_h}{\delta} = 1.62[Re \times Sc \times \left(\frac{d_h}{L}\right)]^{1/3}$ (6)

where d_P is the particle diameter, ρ_p the particle density, ρ_l the liquid viscosity, η the dynamic viscosity, δ the boundary layer thickness calculated by the Leveque equation, u_o the average fluid velocity, and h is the half-channel height. All the calculated velocities and permeation linear velocities of patterned membranes were

plotted as the function of particle size in figure 22. Particle can be deposited on the membrane surface when permeation velocity is larger than total back transport velocity. Therefore, particle with size of lower than 15 μm can be used for comparing deposited mass on the membranes in this cross-flow filtration system.

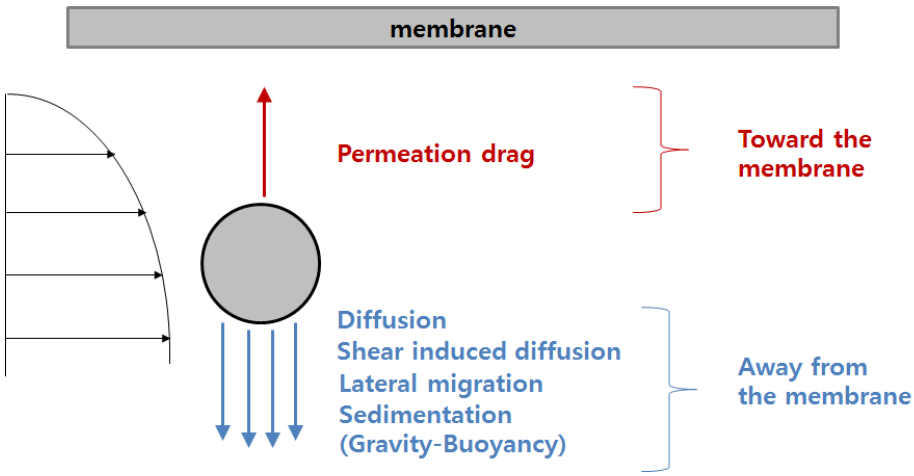

Figure 21. Forces and torques acting on spherical particle suspended in laminar flow system in the vicinity or a flat porous membrane surface.

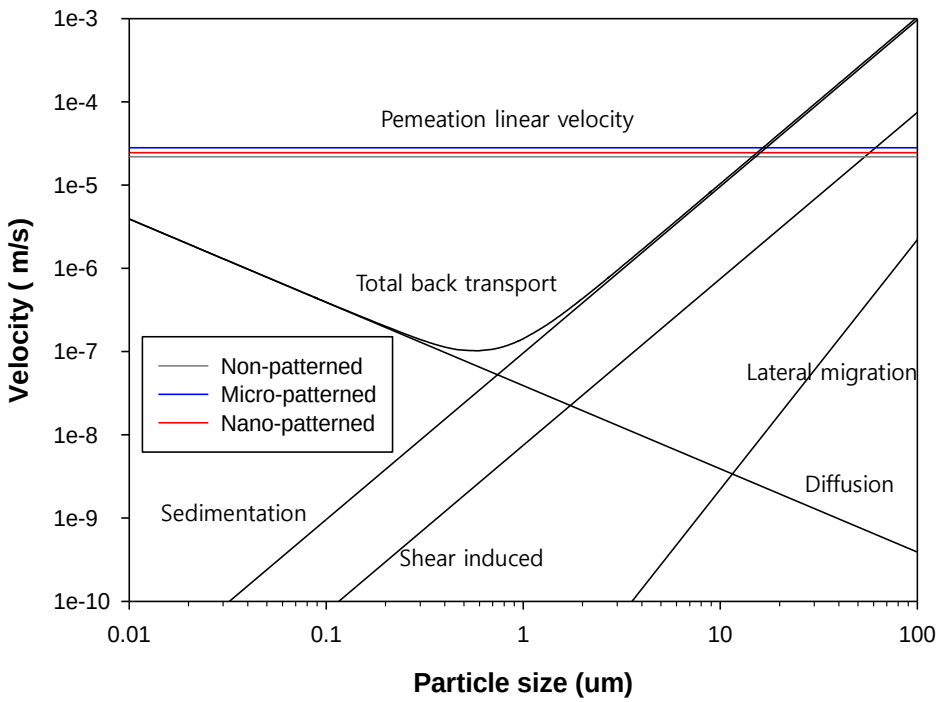

Figure 22. Back transport velocities of the partices and permeation velocities of patterned and non-patterned membranes plotted as function of particle size

IV.6 Particle deposition on patterned membranes.

To observe particle deposition of patterned and non-patterned membranes, we operated cross-flow ultrafiltration system. Each compacted membrane was placed on the module and the feed containing latex particle was circulated at 200 kPa for 2 hr. After colloidal filtration, the mass of deposited latex particles on each membrane was measured using spectrophotometer. Figure 23 shows total data for mass of deposited particles on the membrane surface after the cross flow operation using 0.1, 0.5, 2, and 6 μm particles at the Reynolds number of 15. Also, particle deposition on each membrane is depicted in figure 24.

IV.6.1 0.1 μm colloidal filtration

In the filtration test using 0.1 μm particles, mass of deposited particle on each membrane is similar to each other regardless of a kind of membrane. It means that the effect of pattern on particle deposition might be too little to detach particle from membrane surface in the filtration test using 0.1 μm particles regardless of pattern size. Although shear stress which is induced by surface pattern is well known as a factor to facilitate detachment of the particles, the shear stress can change according to pattern position. Lee et al. reported that local wall shear stress is higher in the upper region of the pattern compared to the lower region as shown in Figure 25. In other words, the lower region corresponding to valley between patterns induces smaller shear stress, so that particle deposition can be caused in the valley. Therefore, the 0.1 μm particles deposited on the valley are likely to stay stably in the region. Moreover, 0.1 μm particles can be trapped between the valleys in the nano-patterned membrane. Once particles are trapped, it is difficult to detach

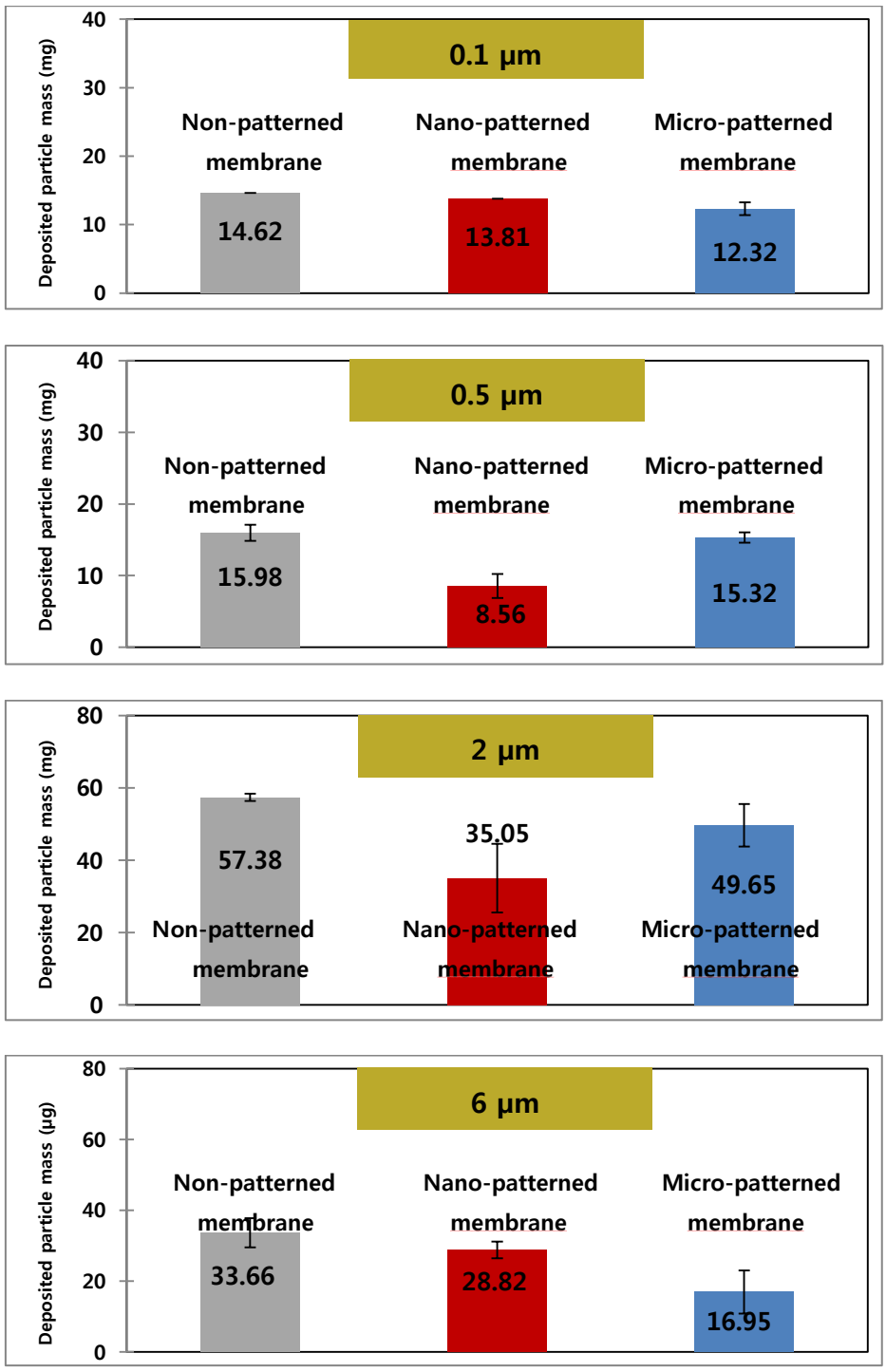

Figure 23. The total mass of deposited particle of nano- and micro- patterned and flat membranes using 0.1, 0.5, 2, and 6 μm sized particle.

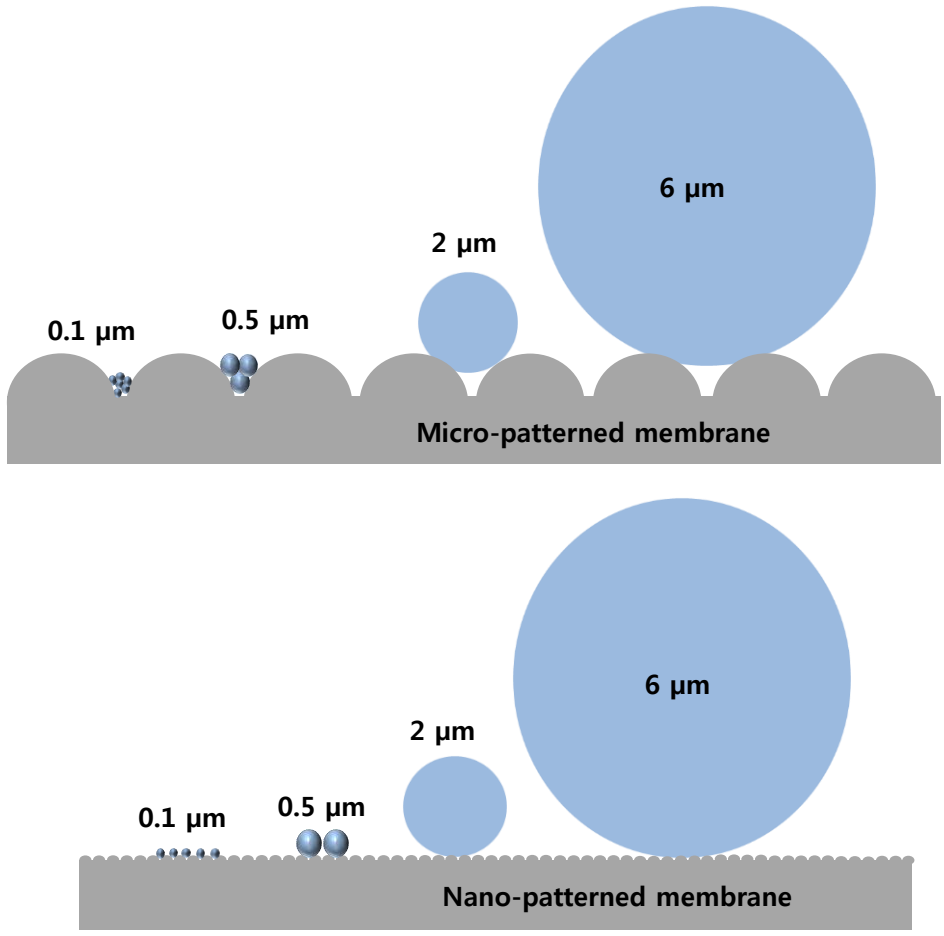

Figure 24. Deposition of various sized particle on nano- and micro- patterned membranes.

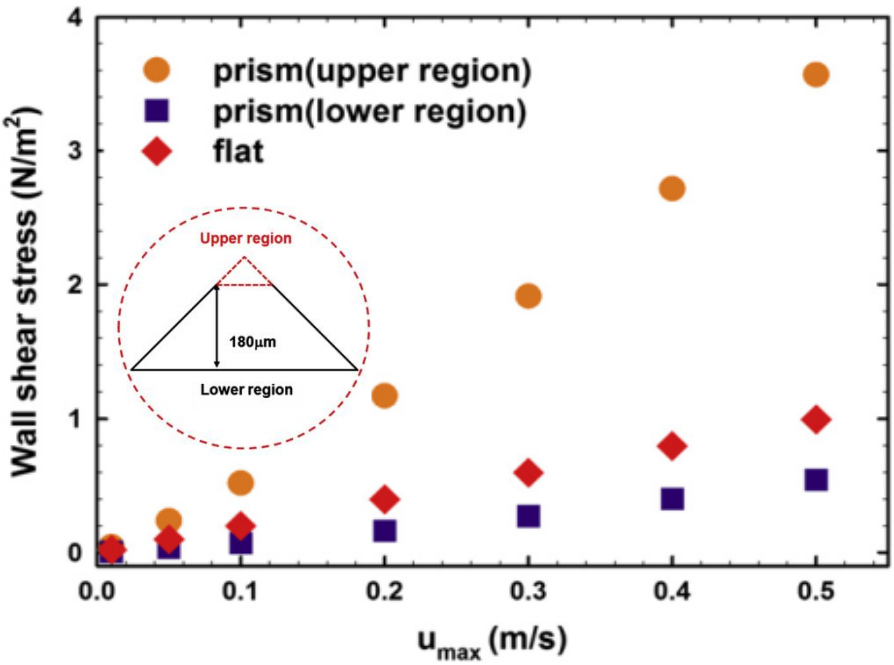

Figure 25. local wall shear stress on the membrane surface as a function of maximum inlet velocity. The circle denotes the results of the upper region in the prism patterned membrane, the square denotes the lower region of prism patterned membrane, and the diamond denotes the flat membrane (Lee, Won et al. 2013). Gksdlf00

deposited particle from membrane surface. According to previous study, the foulants with the similar size to pattern are able to fit between the patterns, which can prolong the retention time of the foulants on the surface. (Whitehead and Verran 2006). In short, it can be difficult to detach particles from the surface of patterned membranes due to low shear region and trapping phenomenon, if the size of particles is less than or equal to the size of pattern.

IV.6.2 0.5 and2 μm particle deposition

The particle deposition behaviors of 0.5 and 2 μm on patterned membrane were similar. The effect of the pattern was more distinct in the filtration test using 0.5 and 2 μm particles unlike the case of 0.1 μm particles. Especially, nano-patterned membrane showed a marked improvement in the inhibition of particle deposition compared to micro-patterned membrane. It resulted from the larger size of particles than that of nano pattern, because 0.5 and 2 μm particles could not be deposited on the lower shear region of nano-patterned membrane and trapped between the nano patterns. On the other hand, 0.5 μm particles could be located on the lower shear region of micro-pattern and 2 μm particles could still be trapped between micro patterns, so that the effect of shear stress induced by micro-patterned membrane was yet insignificant compared to that of nano-patterned membrane.

IV.6.3 6 μm particle deposition

It would be assumed that all the patterned membranes have superior anti-fouling characteristics than non-pattern membrane in the filtration test using 6 μm particles, since the 6 μm particles are too large to be deposited or trapped between patterns. However, the effect of the pattern remarkably appeared only in micro-

patterned membrane. In short, it means that pattern membrane with smaller patterns than particles is not always desirable to the inhibition of particle deposition. For this reason, we examined the correlation between membrane fouling and the ratio of particle size to pattern.

IV.6.4 Correlation between membrane fouling and the ratio of particle to pattern size

To clarify degree of fouling by changing the ratio particle size to pattern size, we plotted the ratio of the deposited particle mass on patterned membranes to that on non-patterned membrane as a function of the size ratio between particle and pattern (Figure 26). In this session, we defined the ratio between particle size and pattern size as R_p.

$$R_p = \frac{Particle\ size}{Pattern\ size}$$

As shown in Figure 26, three kinds of different particle deposition were observed along with R_p values.

In region 1, there was no or little anti-fouling effect on patterned membrane. As discussed in previous session, smaller particle than pattern can be deposited on the valley of patterns where little shear force exists. Additionally, trapping of particle can occur between patterns when pattern size is similar to particle size.

On the other hand, the particle deposition was mitigated on the whole when the value of R_p was located in region 2. If particles are larger than pattern size, particles cannot be placed on lower shear region and trapped between patterns. It means that the particle deposition could be influenced by only pattern including shear stress without the aforementioned side effects caused by the introduction of

pattern.

However, larger R_p than 1 is not always desirable to the inhibition of particle deposition, because required pattern effect to detach deposited particle can differ according to particle size or mass. When particle to pattern size ratio falls in region 3 as depicted in Figure 26, enhanced detachment force by patterns is not yet sufficient to induce particle detachment of particles in systems in region 3. In other words, at a scale in which the particle size is dramatically larger than pattern size, effect of surface pattern is nullified as if the surface had no pattern at all.

This fact suggests that optimum value of R_p is located around 5 (region 2) for the inhibition of particle deposition. Although a quantitative assessment cannot accurately be made with regard to the balancing effects of particle size and pattern size, the results obtained indicates that the dominant factor affecting particle deposition is the existence of side effects such as particle trapping and deposition in lower shear region when the R_p is smaller than 1 whereas it becomes apparent pattern effect occurring between particle and pattern when the R_p is larger than 1.

Pattern size (μm)	2	2	0.11	2	2	0.11	0.11	0.11
Particle size (μm)	0.1	0.5	0.1	2	6	0.5	2	6
R_p	0.05	0.25	0.091	1	3	4.55	18.18	54.54
Relative deposited particle mass	0.84	0.96	0.94	0.87	0.50	0.54	0.61	0.86

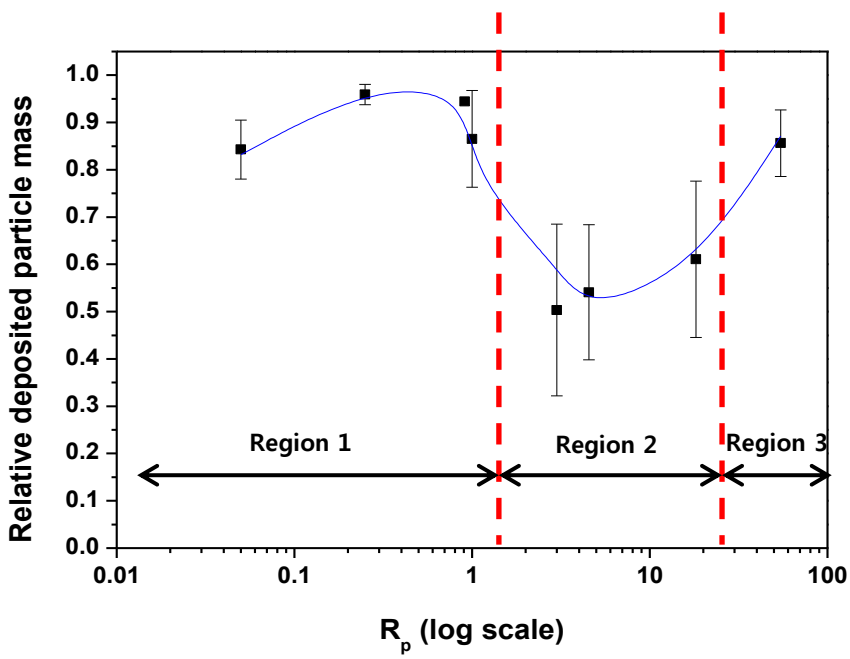

Figure 26. Relative deposited particle mass (deposited particle mass on patterned membrane / non-patterned membrane) by change in R_p

Chapter V

Conclusions

The purpose of this study is to clarify correlation between membrane fouling and the ratio of particle size to pattern. To achieve this, we conducted followings: i) Preparation of UF membranes with nano- and micro- scale pattern ii) Analysis of effect of pattern size on anti-fouling characteristics of patterned membrane by operating cross flow system with latex particle. Based on the results of this study, the following conclusions were made.

- Using hot-embossing NIL method, nano- and micro-scaled patterns were can be successfully introduced on PES UF membranes. By analyzing SEM and AFM images of patterned membrane, the embossing-type patterns with size of 110 nm and 2 μm were regularly formed on the membrane surface.

- Although all the membranes have similar pore size, which is about 10nm, regardless of existence of pattern or pattern size, the nano- and micro-patterned membranes showed higher water permeability than flat membrane. It is inferred that the increase in water permeability was mainly caused by the enlargement of effective surface area due to patterning process.

- The relationship between pattern size and particle size was examined by operating colloidal filtration test using different size of latex particle. To explain particle deposition depending on the relationship, we defined the ratio of particle size to pattern size as R_p. By plotting relative deposited

particle mass on patterned membrane divided by that on non-patterned membrane as function of R_p, we confirmed that optimum value of R_p was shown around 5 for the inhibition of particle deposition. In addition, the obtained results indicate that the dominant factor affecting particle deposition is the existence of side effects such as particle trapping and deposition in lower shear region when the R_p is smaller than 1, whereas it becomes apparent pattern effect occurring between particle and pattern when the R_p is larger than 1.

Reference

Aimar, P., et al. (1990). "A contribution to the translation of retention curves into pore size distributions for sieving membranes." *Journal of Membrane Science* **54**(3): 321-338.

Amirilargani, M., et al. (2010). "Effects of coagulation bath temperature and polyvinylpyrrolidone content on flat sheet asymmetric polyethersulfone membranes." *Polymer Engineering & Science* **50**(5): 885-893.

Arya, R. K. (2013). "Drying Induced Phase Separation." *Journal of Chemical Engineering* **27**(1): 12-20.

Baker, R. W. (2000). *Membrane technology*, Wiley Online Library.

Bansod, P. G., et al. (2012). "Influence Of Ethanol Concentration On The Performance Of Polyethersulfone Ultra Filtration Membranes." *International Journal of ChemTech Research* **4**(4).

Beck, M., et al. (2002). "Improving stamps for 10 nm level wafer scale nanoimprint lithography." *Microelectronic engineering* **61**: 441-448.

Bergmair, I., et al. (2008). "Equalising stamp and substrate deformations in solid parallel-plate UV-based nanoimprint lithography." *Microelectronic engineering* **85**(5): 822-824.

Bikel, M., et al. (2009). "Micropatterned polymer films by vapor-induced phase separation using permeable molds." *ACS applied materials & interfaces* **1**(12): 2856-2861.

Boussu, K., et al. (2006). "Evaluation of self-made nanoporous polyethersulfone membranes, relative to commercial nanofiltration membranes." *Desalination* **200**(1): 416-418.

Chen, C. S., et al. (1997). "Geometric control of cell life and death." *Science* **276**(5317): 1425-1428.

Chou, S. Y., et al. (1995). "Imprint of sub-25 nm vias and trenches in polymers." *Applied physics letters* **67**(21): 3114-3116.

Committee, A. M. T. R. (2005). "Committee Report: Recent Advances and Research Needs in Membrane Fouling (PDF)." *Journal-American Water Works Association* **97**(8): 79-89.

Çulfaz, P. Z., et al. (2011). "Fouling behavior of microstructured hollow fiber membranes in dead-end filtrations: critical flux determination and NMR imaging of particle deposition." *Langmuir* **27**(5): 1643-1652.

Çulfaz, P. Z., et al. (2010). "Microstructured hollow fibers for ultrafiltration." *Journal of Membrane Science* **347**(1): 32-41.

Drews, A. (2010). "Membrane fouling in membrane bioreactors—characterisation, contradictions, cause and cures." *Journal of Membrane Science* **363**(1): 1-28.

Drioli, E. and L. Giorno (2009). Membrane operations: innovative separations and transformations, *Wiley-VCH*.

Gao, H., et al. (2006). "Air cushion press for excellent uniformity, high yield, and fast nanoimprint across a 100 mm field." *Nano letters* **6**(11): 2438-2441.

Hiroshima, H. (2006). "Photo-nanoimprinting using sample-on-flexible-thruster stage." *Japanese journal of applied physics* **45**(6S): 5602.

Hobbs, C., et al. (2006). "Effect of surface roughness on fouling of RO and NF membranes during filtration of a high organic surficial groundwater." *Journal of Water Supply: Research & Technology-AQUA* **55**.

Huang, Y., et al. (2006). "Solvent resistant microfluidic DNA synthesizer." *Lab Chip* **7**(1): 24-26.

Jamshidi Gohari, R., et al. (2013). "Effect of surface pattern formation on membrane fouling and its control in phase inversion process." *Journal of Membrane Science* **446**: 326-331.

Kang, S., et al. (2006). "Effect of membrane surface properties during the fast evaluation of cell attachment." *Separation Science and Technology* **41**(7): 1475-1487.

Kassotis, J., et al. (1985). "Modelling of the pore size distribution of ultrafiltration membranes." *Journal of Membrane Science* **22**(1): 61-76.

Kim, I. C., et al. (2002). "Formation of integrally skinned asymmetric polyetherimide nanofiltration membranes by phase inversion process." *Journal of applied polymer science* **84**(6): 1300-1307.

Kim, S. H., et al. (2007). "Fabrication of photonic crystal structures on light emitting diodes by nanoimprint lithography." *Nanotechnology* **18**(5): 055306.

Lalia, B. S., et al. (2013). "A review on membrane fabrication: Structure, properties and performance relationship." *Desalination* **326**: 77-95.

Lee, H., et al. (2007). "Fabrication of Ge< sub> 2</sub> Sb< sub> 2</sub> Te<

sub> 5</sub> based PRAM device at 60nm scale by using UV nanoimprint lithography." *Microelectronic engineering* **84**(4): 573-576.

Lee, Y. K., et al. (2013). "Flow analysis and fouling on the patterned membrane surface." *Journal of Membrane Science* **427**: 320-325.

Liu, S. X. and J.-T. Kim (2011). "Characterization of surface modification of polyethersulfone membrane." *Journal of adhesion science and technology* **25**(1-3): 193-212.

Mühlberger, M., et al. (2009). "UV-NIL with working stamps made from Ormostamp." *Microelectronic engineering* **86**(4): 691-693.

Maruf, S. H., et al. (2013). "Influence of sub-micron surface patterns on the deposition of model proteins during active filtration." *Journal of Membrane Science* **444**: 420-428.

Maruf, S. H., et al. (2013). "Use of nanoimprinted surface patterns to mitigate colloidal deposition on ultrafiltration membranes." *Journal of Membrane Science* **428**: 598-607.

Masuda, H. and K. Fukuda (1995). "Ordered metal nanohole arrays made by a two-step replication of honeycomb structures of anodic alumina." *Science* **268**(5216): 1466-1468.

Michaels, A. S. (1980). "Analysis and prediction of sieving curves for ultrafiltration membranes: A universal correlation?" *Separation Science and Technology* **15**(6): 1305-1322.

Mulder, M. (1996). Basic Principles of Membrane Technology Second Edition, *Kluwer Academic Pub*.

Park, S.-H., et al. (2006). "Effective fabrication of three-dimensional nano/microstructures in a single step using multilayered stamp." *Applied physics letters* **88**(20): 203105.

Peters, A. M., et al. (2008). "Comparing flat and micro-patterned surfaces: Gas permeation and tensile stress measurements." *Journal of Membrane Science* **320**(1): 173-178.

Pinnau, I. and B. D. Freeman (2000). "Membrane formation and modification."

Platzgummer, E., et al. (2007). Projection maskless patterning (PMLP) for the fabrication of leading-edge complex masks and nano-imprint templates. 27th Annual BACUS Symposium on Photomask Technology, International Society for Optics and Photonics.

Reuvers, A. and C. Smolders (1987). "Formation of membranes by means of

immersion precipitation: Part II. the mechanism of formation of membranes prepared from the system cellulose acetate-acetone-water." *Journal of Membrane Science* **34**(1): 67-86.

Riedl, K., et al. (1998). "Influence of membrane structure on fouling layer morphology during apple juice clarification." *Journal of Membrane Science* **139**(2): 155-166.

Schift, H. and A. Kristensen (2010). Nanoimprint Lithography–Patterning of Resists Using Molding. *Springer Handbook of Nanotechnology*, Springer**:** 271-312.

Shojaie, S. S., et al. (1994). "Dense polymer film and membrane formation via the dry-cast process Part II. Model validation and morphological studies." *Journal of Membrane Science* **94**(1): 281-298.

Singh, S., et al. (1998). "Membrane characterization by solute transport and atomic force microscopy." *Journal of Membrane Science* **142**(1): 111-127.

Smolders, C., et al. (1992). "Microstructures in phase-inversion membranes. Part 1. Formation of macrovoids." *Journal of Membrane Science* **73**(2): 259-275.

Strathmann, H., et al. (1975). "The formation mechanism of asymmetric membranes." *Desalination* **16**(2): 179-203.

Truong, T. T., et al. (2007). "Soft lithography using acryloxy perfluoropolyether composite stamps." *Langmuir* **23**(5): 2898-2905.

Vogelaar, L., et al. (2003). "Phase separation micromolding—PSμM." *Advanced Materials* **15**(16): 1385-1389.

Vogler, M., et al. (2007). "Development of a novel, low-viscosity UV-curable polymer system for UV-nanoimprint lithography." *Microelectronic engineering* **84**(5): 984-988.

Vrijenhoek, E. M., et al. (2001). "Influence of membrane surface properties on initial rate of colloidal fouling of reverse osmosis and nanofiltration membranes." *Journal of Membrane Science* **188**(1): 115-128.

Whitehead, K. A. and J. Verran (2006). "The effect of surface topography on the retention of microorganisms." *Food and bioproducts processing* **84**(4): 253-259.

Won, Y.-J., et al. (2012). "Preparation and application of patterned membranes for wastewater treatment." *Environmental science & technology* **46**(20): 11021-11027.

Wu, W., et al. (2005). "One-kilobit cross-bar molecular memory circuits at 30-nm half-pitch fabricated by nanoimprint lithography." *Applied Physics A* **80**(6): 1173-1178.

Yildirim, M. H., et al. (2010). "Micro-patterned Nafion membranes for direct methanol fuel cell applications." *Journal of Membrane Science* **349**(1): 231-236.

Zhang, W. and S. Y. Chou (2001). "Multilevel nanoimprint lithography with submicron alignment over 4 in. Si wafers." *Applied physics letters* **79**(6): 845-847.

Zhou, W., et al. (2011). "Nanoimprint Lithography: A Processing Technique for Nanofabrication Advancement." *Nano-Micro Letters* **3**(2).

국문초록

분리막을 이용한 수처리 공정은 양질의 처리수를 확보할 수 있는 장점이 있으나, 분리막 표면에 발생하는 막오염으로 인해 투수도가 낮아지고 운전비용이 증가하는 문제점이 있다. 이러한 분리막 오염을 저감하기 위한 여러 가지 방안 중 분리막 표면에 패턴을 도입함으로써 막오염을 저감시킨 사례가 최근 보고되었고, 패턴 분리막이 차세대 분리막을 위한 대안으로서 가능성을 가지고 있다는 것이 확인되었다. 하지만 기존의 연구에서는 패턴형 분리막에서 막오염이 저감될 수 있다는 가능성만 제시했을 뿐, 실제 유입수 내의 부유물질이 표면 패턴에서 어떤 방식으로 거동함으로써 막오염이 저감되는지에 대한 깊이 있는 연구는 아직 진행된 바 없다. 따라서 이 연구에서는 막오염 저감을 결정하는데 패턴과 입자크기 간의 비율이 미치는 영향을 살펴보기 위해 i) 다양한 크기 (나노 그리고 마이크로 크기)의 패턴을 가지는 패턴형 분리막을 제조하고 ii) 패턴 크기에 따른 다양한 크기의 입자 (0.1, 0.5, 2, 6 μm) 부착을 비교하여 패턴크기와 입자크기의 상관관계가 막오염에 미치는 영향을 조사하였다.

먼저, 본 연구에서는 나노 임프린트 기법을 이용하여 기존에 연구된 패턴 모양과는 다른 엠보싱 모양의 패턴을 나노 그리고 마이크로 크기로 PES UF 분리막에 전사하였다. 특히 나노 패턴형 분리막의 경우, 기존에는 구현된 바 없는 정교한 나노 크기의 패턴을 AAO를 마스터몰

드로 하여 구현하였다. 또한. AFM과 SEM 이미지 분석을 통해 나노 패턴은 110 nm, 마이크로 패턴은 2 μm 의 패턴이 형성되었음을 확인하였다. 이렇게 준비한 패턴형 분리막은 패턴크기와 상관없이 기공크기가 10 nm 정도로 유사하였지만, 패턴도입에 의한 유효 막 면적의 증가로 인해 평판형 분리막 대비 10 – 30 %의 높은 투수도를 보였다.

다음으로, 다양한 크기의 입자 투과 실험을 통하여 패턴형 분리막에서 입자와 패턴 크기의 비가 미치는 막오염에 미치는 영향을 관찰하였다. 이번 연구에서 패턴의 크기에 대한 입자의 크기 비율을 R_p 라 정의하였고 이 값에 따른 입자들의 부착 양을 조사, 비교하였다. 이를 통해, 패턴과 입자 크기의 비에 따른 막 오염의 변화를 도시화 할 수 있었으며, 유입수 내의 입자의 크기 범위가 0.1 – 6 μm 인 경우 R_p 값이 5 부근에서 막오염 억제가 가장 효과적임을 확인하였다. 이는 입자들이 패턴 사이에 들어가 비가역적으로 침착되거나 개재 고립이 발생하는 다른 구간에 비해, 해당 구간에서는 패턴 주변에서의 유동변화로 인한 탈착 유도가 충분히 나타나기 때문으로 해석된다.

이번 실험에서 나노 크기에 해당하는 정교한 패턴을 갖는 나노 패턴형 분리막을 제작 할 수 있음을 확인하였고, 다양한 크기의 입자를 이용한 입자투과 실험을 통해 패턴과 입자크기 간의 비율이 막오염 저감을 결정하는 주요한 인자일 수 있다는 가능성을 보여주었다.

주요어 : 분리막공정, 패턴형 분리막, 막오염 제어, 리소그래피, 입자 부착, 나노 패턴

학번 : 2012-20971